

Bassoon controls synaptic vesicle release via regulation of presynaptic phosphorylation and cAMP

Carolina Montenegro-Venegas^{1,2,3} , Debarpan Guhathakurta⁴ , Eneko Pina-Fernandez⁵, Maria Andres-Alonso⁵ , Florian Plattner⁶, Eckart D Gundelfinger^{1,2,3}  & Anna Fejtova^{1,4,5,*} 

Abstract

Neuronal presynaptic terminals contain hundreds of neurotransmitter-filled synaptic vesicles (SVs). The morphologically uniform SVs differ in their release competence segregating into functional pools that differentially contribute to neurotransmission. The presynaptic scaffold bassoon is required for neurotransmission, but the underlying molecular mechanisms are unknown. We report that glutamatergic synapses lacking bassoon feature decreased SV release competence and increased resting pool of SVs as assessed by imaging of SV release in cultured neurons. CDK5/calcineurin and cAMP/PKA presynaptic signalling are dysregulated, resulting in an aberrant phosphorylation of their downstream effectors synapsin1 and SNAP25, well-known regulators of SV release competence. An acute pharmacological restoration of physiological CDK5 and cAMP/PKA activity fully normalises the SV pools in neurons lacking bassoon. Finally, we demonstrate that CDK5-dependent regulation of PDE4 activity interacts with cAMP/PKA signalling and thereby controls SV release competence. These data reveal that bassoon organises SV pools in glutamatergic synapses via regulation of presynaptic phosphorylation and cAMP homeostasis and indicate a role of CDK5/PDE4/cAMP axis in the control of neurotransmitter release.

Keywords Bassoon; PDE4; neuromodulation; neurotransmission; synaptic vesicle recycling

Subject Categories Membrane & Trafficking; Neuroscience; Signal Transduction

DOI 10.15252/embr.202153659 | Received 23 July 2021 | Revised 23 May 2022 |

Accepted 1 June 2022 | Published online 29 June 2022

EMBO Reports (2022) 23: e53659

Introduction

Synapses are contact sites between neurons, where communication between presynaptic and postsynaptic neuron occur by means of

electrochemical neurotransmission. Within the presynapse, the neurotransmitter is stored in small synaptic vesicles (SVs) and released upon their fusion with the presynaptic plasma membrane. After their fusion, the membrane and protein components of SVs are retrieved by compensatory endocytosis, and SVs are refilled with neurotransmitters and recycled (Sudhof, 2004). This SV cycle ensures the long-term structural and functional integrity of the presynaptic compartment (Chanaday *et al*, 2019; Bonnycastle *et al*, 2020). SVs, albeit structurally identical, differ in their release competence (i.e. capability to fuse with presynaptic plasma membrane upon stimulus) and display varying kinetics of release in response to stimuli, resulting in three distinct SV pools (Rizzoli & Betz, 2005; Denker & Rizzoli, 2010; Alabi & Tsien, 2012). The readily releasable pool (RRP) contains vesicles that discharge immediately upon stimulation and correspond morphologically to the docked SVs, which are in contact with the plasma membrane of the presynaptic active zone (Schikorski & Stevens, 2001). The recycling pool (RP) is a source of releasable vesicles that can replenish RRP during prolonged stimulation. Both RRP and RP together form the total recycling pool (TRP). A large proportion of SVs is unable to undergo release under physiological conditions and form the reserve pool (ResP) of SVs. The size of RRP and RP at a given synapse decisively shapes its physiological properties. RRP size determines together with release probabilities of individual SVs synaptic release probability, whereas the size of the RP influences the replenishment of SVs during stimulation trains (Alabi & Tsien, 2012). The release competence of SVs and thus their assignment to the functional pools is under the control of intracellular signalling pathways. Cyclin-dependent kinase 5 (CDK5)/calcineurin signalling plays a crucial role in the regulation of the transition of SVs between the RP and ResP (Kim & Ryan, 2010), while cyclic adenosine monophosphate (cAMP)/cAMP-dependent protein kinase A (PKA) signalling was linked to the control of RRP (Lonart *et al*, 1998; Nagy *et al*, 2004). Phosphoproteins of the synapsin (Syn) family are SV-associated proteins that integrate the signalling from kinases and phosphatases of

1 Department of Neurochemistry and Molecular Biology, Leibniz Institute for Neurobiology, Magdeburg, Germany

2 Center for Behavioral Brain Sciences (CBBS), Magdeburg, Germany

3 Institute for Pharmacology and Toxicology, Medical Faculty, Otto von Guericke University, Magdeburg, Germany

4 Molecular Psychiatry, Department of Psychiatry and Psychotherapy, Universitätsklinikum Erlangen, Friedrich-Alexander-Universität Erlangen-Nürnberg, Erlangen, Germany

5 RG Presynaptic Plasticity, Leibniz Institute for Neurobiology, Magdeburg, Germany

6 Neuro-Research, Houston, TX, USA

*Corresponding author. Tel: +49 9131 85 46155; E-mail: anna.fejtova@uk-erlangen.de

multiple pathways to control the plasticity of neurotransmitter release. Syn is critical for the formation and maintenance of the SV cluster above the presynaptic active zone (Pieribone *et al*, 1995). Depending on its phosphorylation state, Syn oligomerises and interacts with SVs and with the actin cytoskeleton, which in turn modulates dynamic SV clustering (Chi *et al*, 2003; Cesca *et al*, 2010). Syn phosphorylation by cAMP/PKA signalling increases the SV mobilisation. It allows the transition of vesicles from RP to the RRP but also promotes an increased exchange of SVs between adjacent synaptic varicosities along axons (Menegon *et al*, 2006; Valente *et al*, 2012; Patzke *et al*, 2019; Chenouard *et al*, 2020). Phosphorylation of Syn by CDK5 enhances its association with actin filaments and mediates a shift of SVs from RP to ResP (Verstegen *et al*, 2014). Interference with phosphorylation of Syn by PKA and CDK5, respectively, affects the presynaptic short-term and homeostatic plasticity highlighting the importance of dynamic phosphorylation at presynapse for physiological regulation of neurotransmission (Menegon *et al*, 2006; Valente *et al*, 2012; Verstegen *et al*, 2014).

Bassoon (Bsn) is a large scaffolding protein localised exclusively at the active zone of neurotransmitter release (Dieck *et al*, 1998). It plays a key role in the organisation and maintenance of the presynaptic release apparatus (Gundelfinger *et al*, 2015). Mice with a deletion of the central part of Bsn show generalised seizures and impaired synaptic structure and function (Altrock *et al*, 2003; Dick *et al*, 2003). Bsn was shown to coordinate the recruitment of specific presynaptic voltage-gated calcium channels to the active zone via its interaction with RIM-binding proteins (Davydova *et al*, 2014). Therefore, the Cav2.1 and Cav1.3 channels, respectively, are less abundant in cortico-hippocampal glutamatergic synapses or cochlear and retinal ribbon synapses of Bsn mutants (Frank *et al*, 2010; Davydova *et al*, 2014; Babai *et al*, 2019; Ryl *et al*, 2021). Investigations of mouse strains expressing shortened or null Bsn alleles detected reduced RRP and slower vesicular replenishment in glutamatergic synapses of cultured hippocampal neurons, cerebellar mossy fibres, photoreceptors, cochlear inner hair cells and auditory nerve fibres (Altrock *et al*, 2003; Khimich *et al*, 2005; Frank *et al*, 2010; Hallermann *et al*, 2010; Jing *et al*, 2013; Mendoza Schulz *et al*, 2014; Babai *et al*, 2019, 2021; Ryl *et al*, 2021). The morphological analyses also pointed towards a role of Bsn (and its paralogue Piccolo) in the SV clustering and RRP regulation (Altrock *et al*, 2003; Mukherjee *et al*, 2010; Mendoza Schulz *et al*, 2014; Ackermann *et al*, 2019; Hoffmann-Conaway *et al*, 2020). However, the molecular basis for the role of Bsn in the regulation of RRP size and/or release site replenishment remained unclear.

In this study, we investigated the cellular signalling that drives the dynamic regulation of SV recycling using *in vivo* imaging of hippocampal neurons derived from Bsn mutant mice (Bsn^{GT}). We observed a reduced size of RRP and TRP and a significant drop in the overall release competence of SVs in glutamatergic synapses lacking Bsn. These phenotypes were associated with a dysregulation of CDK5/calceinurin balance and cAMP/PKA presynaptic signalling. Acute pharmacological treatment that restored physiological signalling fully normalised the SV release competence in Bsn^{GT} neurons indicating a causal role of aberrant signalling in the loss of release competence in the absence of Bsn. Finally, our data uncovered a key role of CDK5-dependent regulation of PDE4 in the control of SV pools upstream of cAMP/PKA signalling.

Results

Deletion of Bsn restricts recycling competence of SVs

Previous studies indicated changes in the size of RRP in the absence of Bsn in various types of synapses. However, to date, the mechanistic understanding of this phenomenon is missing. To monitor SV exocytosis in living neurons, we expressed the pH-sensitive probe, synaptophluorin-dimer2 (sypHy), using lentiviral vectors in cultured hippocampal neurons that were derived from Bsn^{GT} animals, where Bsn expression was abolished by insertion of a gene-trap cassette (Hallermann *et al*, 2010) and from their WT littermates. In sypHy, pH-sensitive GFP is inserted in the luminal domain of the integral SV protein synaptophysin. The fluorescence of sypHy is quenched by the acidic milieu of SVs, it increases after SV fusion and exposure to the neutral media and decreases again upon SVs endocytosis and re-acidification, which allows monitoring of SV recycling. The red fluorescent dimer2 inserted within the cytoplasmic part of synaptophysin permits the identification of sypHy-expressing cells at rest (Rose *et al*, 2013). We utilised an established stimulation protocol consisting of 40 action potentials (AP) at 20 Hz to drive the fusion of docked SVs (corresponding to RRP) and 900 AP at 20 Hz to release all release-competent SVs (TRP) (Burrone *et al*, 2006). To prevent re-acidification of endocytosed SVs that occurs concomitantly with SV exocytosis during stimulation experiments were performed in the presence of bafilomycin A, a vesicular proton pump inhibitor. Under these conditions, all vesicles that once underwent exocytosis remain visible (Fig 1A and B). We detected significantly lower RRP and TRP in Bsn^{GT} compared with WT neurons (Fig 1A–C and E; RRP: WT 0.13 ± 0.01 , Bsn^{GT} 0.08 ± 0.01 ; TRP: WT 0.41 ± 0.01 , Bsn^{GT} 0.29 ± 0.01). Application of ammonium chloride, which alkalinizes the SV and un-quenches all sypHy-expressing SVs that do not recycle, revealed a rise in the ResP in Bsn^{GT} (Fig 1A and B; ResP: WT 0.60 ± 0.013 , Bsn^{GT} 0.71 ± 0.02). Quantification of the total synaptic intensity of sypHy upon unquenching also confirmed no changes in its synaptic expression levels between Bsn^{GT} and WT neurons (Fig 1A; WT $1,061 \pm 143.8$ AU, Bsn^{GT} $1,041 \pm 90.2$ AU). A clear-cut left shift in the bell-shaped frequency distribution of the response amplitude was evident in Bsn^{GT} upon 40 APs (Fig 1D) and 900APs (Fig 1F) confirming overall lower response magnitude in the Bsn^{GT} neurons compared with WT. This argues against functional inactivation of a fraction of synapses upon deletion of Bsn reported in earlier studies and for overall impairment (Altrock *et al*, 2003). Collectively, these experiments indicate a role of Bsn in the regulation of release competence of SV and their distribution to RRP and RP.

The hippocampal neuron cultures used in these experiments contain predominantly excitatory pyramidal cells (Kaech *et al*, 2012). To assess the SV recycling specifically in excitatory and inhibitory neurons we combined labelling of active synapses in living neurons using a fluorophore-coupled anti-synaptotagmin1 antibody (Syt1Ab) with postfixation synapse type-specific immunostaining. This Syt1Ab antibody recognises the luminal domain of the integral SV protein Syt1. If added to the media of living cells, it can access its epitope only after fusion of SV with the plasma membrane, when the extracellular media contacts the lumen of SV (Kraszewski *et al*, 1995; Lazarevic *et al*, 2011, 2017). First, we performed Syt1Ab labelling in living neurons without any further

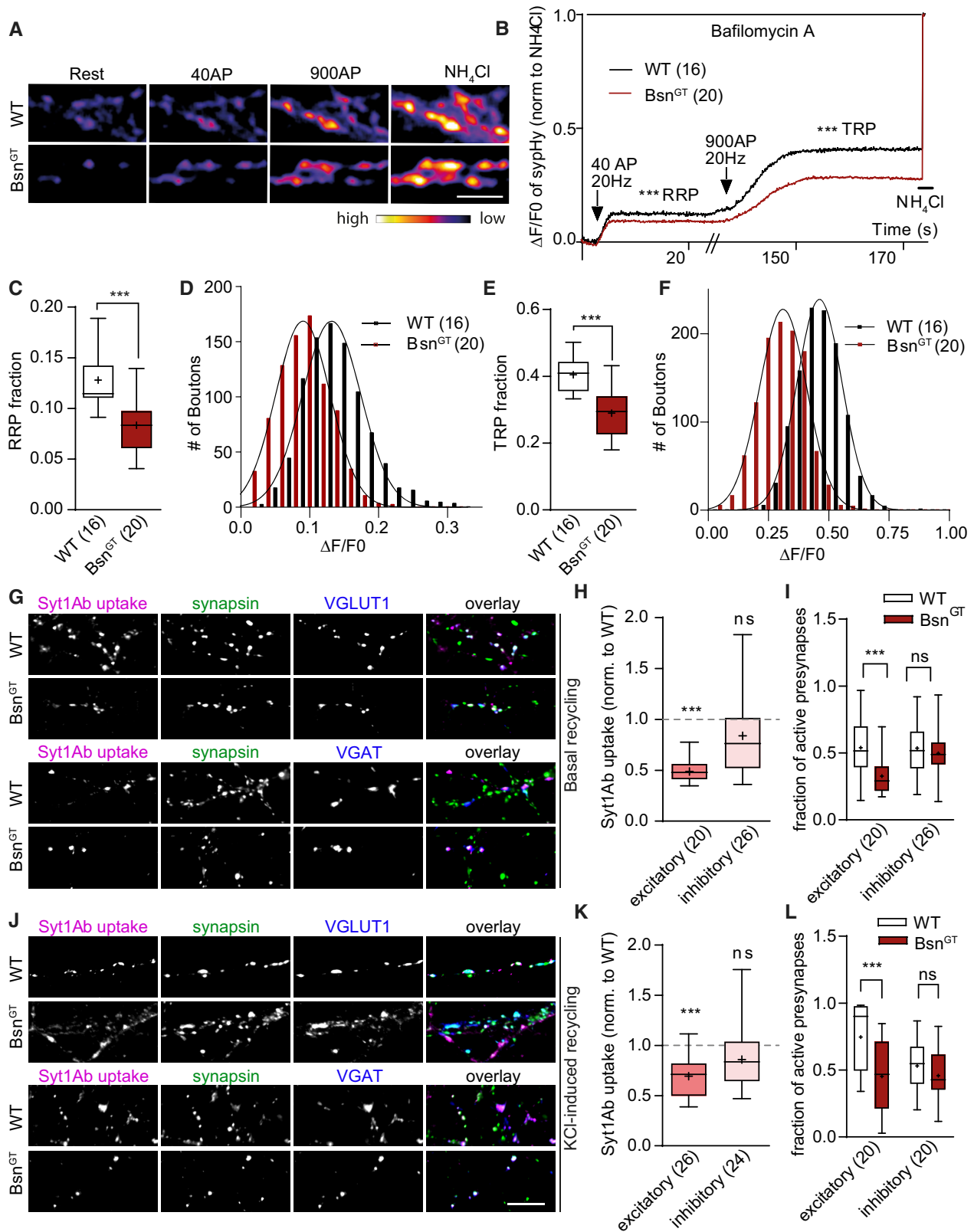


Figure 1.

(Correction added on June 28th 2022, after first online publication: figure 1D exchanged, because the color code was wrong).

Figure 1. Bassoon deletion affects the release competence of SV at glutamatergic synapse.

- A Representative pseudo colour images of sypHy fluorescence in WT and Bsn^{GT} hippocampal neurons at rest, upon stimulation with 40 and 900 APs at 20 Hz (in the presence of bafilomycin A1) and upon application of NH₄Cl to visualise SVs that were refractory to electrical stimulation.
- B Average traces of the normalised fluorescence change ($\Delta F/F_0$) of sypHy in WT (black) and Bsn^{GT} (red) neurons as described in (A). Intensities were normalised to the peak of NH₄Cl response.
- C Quantifications of mean RRP fraction in WT and Bsn^{GT}.
- D Frequency distribution histograms of the response amplitudes of 1,050 individual synaptic puncta (from six independent experiments) to stimulation with 40 AP. The distribution is shifted to lower values in Bsn^{GT}.
- E Quantifications of mean TRP fraction in WT and Bsn^{GT}.
- F Frequency distribution histograms of synaptic response amplitudes in Bsn^{GT} and WT neurons stimulated with 900 AP. Note the shift in distribution between genotypes.
- G Representative images of Syt1Ab uptake (magenta) driven by endogenous network activity in hippocampal neurons (18 DIV) from WT and Bsn^{GT} mice. VGLUT1 (green) marks excitatory presynapses (upper panels) and VGAT the inhibitory ones (lower panels).
- H Quantification of normalised IF of Syt1Ab uptake in excitatory (red boxes) and inhibitory (pink boxes) synapses on experiments in (G).
- I Quantification of the fraction of active (Syt1Ab-labelled) excitatory and inhibitory synapses on experiments illustrated in (G).
- J Representative images of Syt1Ab uptake (magenta) upon depolarization with 50 mM KCl. Identical cultures and staining were applied as in (G).
- K Quantification of normalised IF of Syt1Ab uptake on experiments from (J).
- L Quantification of the fraction of active excitatory and inhibitory synapses in (J).

Data information: In the plots, the interquartile range and median are depicted as boxes, minimal and maximal values as whiskers, and + indicates mean. In the frequency distribution histograms (D and F) black lines depict superimposed Gaussian fits for each group. The dashed lines in (H) and (K) depict IF in WT that were used for normalisation. The sample size *n* (in parentheses) corresponds to the number of analysed imaging experiments (B, C, E) or to the number of analysed images (G, J). In (D) and (F), the data of 1,050 synapses per genotype were processed. Data is obtained from 6 (A–F) or 3 (G–L) independent culture preparations. Significance was assessed with the Student's *t*-test; ****P* < 0.001. Scale bar is 2 μ m in (A) and 5 μ m in (G) and (J).

manipulations to monitor SV recycling driven by endogenous neuronal activity (Fig 1G). The excitatory synapses were assessed as Syt1Ab-labelled puncta positive for synapsin and vesicular glutamate transporter 1 (VGLUT1) immunoreactivity and inhibitory synapses as puncta co-labelled for synapsin and vesicular GABA transporter (VGAT) (Fig 1G). Syt1Ab uptake driven by basal network activity was significantly lower in Bsn^{GT} excitatory presynapses, and no significant difference was seen in inhibitory boutons (Fig 1G and H; exc: WT 1.00 ± 0.08 , Bsn^{GT} 0.49 ± 0.02 ; inh: WT 1.00 ± 0.07 , Bsn^{GT} 0.84 ± 0.08). To assess the total recycling pool in both synapse types, we performed Syt1Ab labelling during depolarization induced by a brief application of 50 mM KCl, which leads to the release of the total recycling pool of SV (TRP) (Harata *et al*, 2001). Depolarization-induced Syt1Ab uptake was significantly decreased in the excitatory but not in the inhibitory synapses in neurons derived from Bsn^{GT} animals (Fig 1J and K; exc: WT 1.00 ± 0.07 , Bsn^{GT} 0.69 ± 0.04 ; inh: WT 1.00 ± 0.06 , Bsn^{GT} 0.86 ± 0.07).

Postfixation labelling of neurons with a general synaptic marker after Syt1Ab uptake also enabled us to quantify the number of active vs. silent presynapses, i.e. presynapses competent for SV release and recycling under basal network activity or upon chemical depolarization (Moulder *et al*, 2010). The fraction of active glutamatergic synapses, defined as VGLUT1-positive puncta with detectable immunofluorescence (IF) of Syt1Ab uptake, was reduced by 40% in Bsn^{GT} neurons under basal conditions, indicating a higher proportion of silent (i.e. release incompetent) presynapses (Fig 1I; WT 0.54 ± 0.05 , Bsn^{GT} 0.33 ± 0.03). The number of glutamatergic synapses capable of release upon KCl-induced depolarization was also decreased in Bsn^{GT} neurons compared with the WT (Fig 1L; WT 0.75 ± 0.05 , Bsn^{GT} 0.45 ± 0.05). No significant differences in number of release-competent inhibitory, i.e. VGAT and synapsin-positive, synapses were detected (Fig 1I and L; basal: WT 0.55 ± 0.05 , Bsn^{GT} 0.50 ± 0.04 ; KCl: WT 0.53 ± 0.03 , Bsn^{GT} 0.46 ± 0.04). These analyses indicate that loss of Bsn affects the SV release competence predominantly at glutamatergic synapses.

One plausible explanation for the lower release competence of SV could be a change in the expression of synaptic proteins linked to the regulation of synaptic release competence in the absence of Bsn. Indeed, previous studies reported a lower synaptic abundance of RIM or Munc13 and an increased abundance of piccolo (Pclo) upon deletion of Bsn (Altrock *et al*, 2003; Davydova *et al*, 2014; Montenegro-Venegas *et al*, 2021). Therefore, we quantified the synaptic abundance of Munc13 and Pclo in WT and Bsn^{GT} excitatory and inhibitory synapses (Fig EV1A and C). The quantification revealed significant decrease and increase, of immunoreactivity for Munc13-1 and Pclo, respectively, in both excitatory and inhibitory synapses (Fig EV1B and D; Munc13: exc: WT 1.00 ± 0.03 , Bsn^{GT} 0.77 ± 0.02 ; inh: WT 1.00 ± 0.04 , Bsn^{GT} 0.79 ± 0.03 ; Pclo: exc: WT 1.00 ± 0.03 , Bsn^{GT} 1.48 ± 0.04 ; inh: WT 1.00 ± 0.04 , Bsn^{GT} 1.24 ± 0.04). Thus, the synapse type-specific defect in SV release competence cannot be explained just by changes in abundance of Munc13-1 or Pclo upon deletion of Bsn.

CDK5 activity is increased in Bsn^{GT} and uncoupled from regulation by neuronal activity

CDK5 plays an important role in the regulation of release competence of SVs, especially via dynamic recruitment of SVs from the RP and to the ResP (Kim & Ryan, 2010, 2013; Verstegen *et al*, 2014). To assess the potential involvement of CDK5 in the shift of SV from recycling to resting pool that we observed in Bsn^{GT} neurons, we pharmacologically interfered with the activity of this enzyme in WT and Bsn^{GT} neurons. In accordance with the reported role of CDK5, we observed a significant increase in the fraction of RRP and TRP in WT neurons after acute inhibition of CDK5 with roscovitine (100 μ M, 30 min). The analyses of data revealed that roscovitine increased RRP by 68% and TRP by 57% in Bsn^{GT} but only by 38% (RRP) and 29% (TRP) in WT (Fig 2A, B and E; WT vs. Bsn^{GT}; RRP 138 ± 9 vs. 168 ± 10 %; TRP: 129 ± 5 vs. 157 ± 7 %). Importantly, the roscovitine treatment restored RRP and TRP

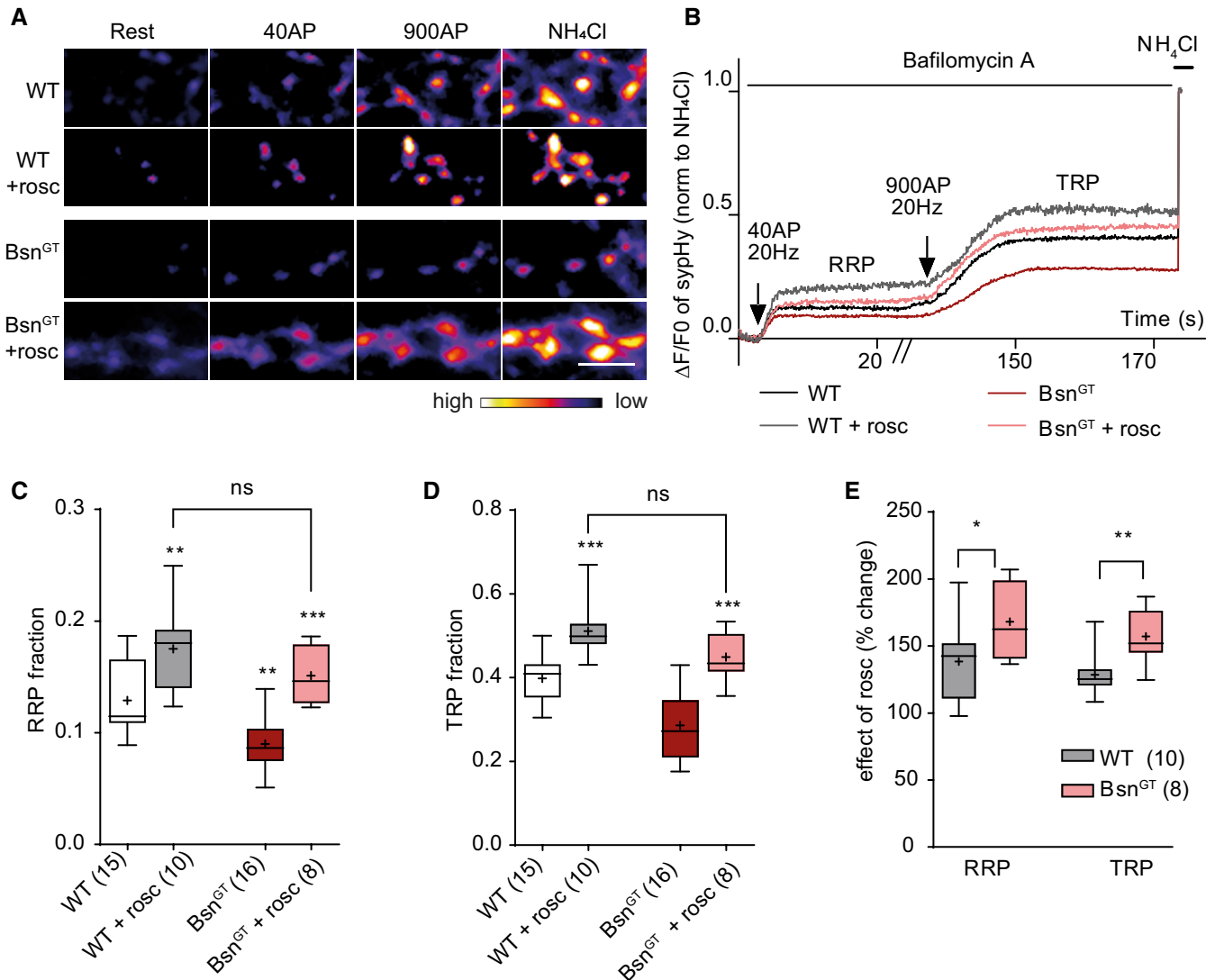


Figure 2. Inhibition of CDK5 activity normalises SV pools in Bsn^{GT} neurons.

A, B Representative pseudo colour images (A) and average traces (B) of synHy fluorescence plotted for WT and Bsn^{GT} neurons treated with a CDK5 inhibitor roscovitine (rosc, 100 μM, grey and pink trace) or vehicle (black and red trace) for 30 min before stimulation with 40 and 900 APs in the presence of bafilomycin A.

C, D Plots show mean values of RRP (C) and TRP (D) fraction for both genotypes before and after treatment.

E Roscovitine treatment has a significantly higher effect on RRP and TRP in Bsn^{GT} neurons compared with WT.

Data information: *n* corresponding to the number of imaging experiments done on four independent cell preparations is given in brackets for each analysis. In the plots, the interquartile range and median are depicted as boxes, minimal and maximal values as whiskers, and + indicates mean. Significance was assessed by two-way ANOVA with the Tukey's multiple comparison test (C, D) and by the Student's *t*-test (E) **P* ≤ 0.05, ***P* < 0.01, ****P* < 0.001. Scale bar is 2 μm.

fractions in Bsn^{GT} neurons to levels similar to treated WT neurons (Fig 2B–D; RRP: WT 0.13 ± 0.01, WT + roscovitine 0.18 ± 0.01, Bsn^{GT} 0.09 ± 0.01, Bsn^{GT} + roscovitine 0.15 ± 0.01; TRP: WT 0.40 ± 0.01, WT + roscovitine 0.51 ± 0.02, Bsn^{GT} 0.29 ± 0.02, Bsn^{GT} + roscovitine 0.45 ± 0.02). This indicates that an elevated activity of CDK5 possibly contributes to the changes in SV pools in Bsn^{GT} neurons.

An important substrate of CDK5 in the context of regulation of SV recycling is the Ser551 of SV-associated protein synapsin1 (Syn1) (Verstegen *et al*, 2014). Phosphorylation at Ser551 of Syn1 (pSer551Syn1) enhances the binding of Syn1 to F-actin, promotes a

shift of SVs to the ResP, and thereby, it restricts SV recycling (Fig 3D) (Verstegen *et al*, 2014). To address whether deregulation of CDK5-dependent pSer551Syn1 underlies the changes in SV pools in Bsn^{GT} neurons we utilised the previously published phospho-specific antibody (Verstegen *et al*, 2014). We detected significantly higher levels of pSer551Syn1 in P2 fractions of hippocampal lysates from Bsn^{GT} mice than in WT, while the total expression levels of Syn1 were unchanged (Fig 3A–C; pSer551Syn1/Syn1: WT 1.00 ± 0.14, Bsn^{GT} 1.32 ± 0.12; Syn1: WT 1.00 ± 0.14, Bsn^{GT} 1.16 ± 0.14). Next, we used this antibody to visualise the abundance of pSer551Syn1 in individual synapses in cultured WT and Bsn^{GT}

neurons. We detected a significantly higher pSer551Syn1 IF intensity in synapses of neurons from Bsn^{GT} compared with the WT, while the total expression of Syn1 did not differ between genotypes (Fig 3E and F; WT 1.00 ± 0.06, Bsn^{GT} 1.55 ± 0.08). Importantly, the pSer551Syn1 immunoreactivity was dramatically decreased in WT terminals upon treatment with roscovitine, confirming the specificity of the antibody (Fig 3E and F; 0.43 ± 0.03). In the next step, we quantified the abundance of total Syn1 and pSer551Syn1 in excitatory synapses labelled against VGLUT1 and in inhibitory synapses labelled against VGAT (Fig EV2A). Expression of Syn1 did not differ between Bsn^{GT} and WT in neither excitatory nor inhibitory synapses (Fig EV2B). However, the situation was different for pSer551Syn1. While IF intensity of pSer551Syn1 labelling was significantly increased in excitatory synapses, it was unchanged in inhibitory ones (Fig EV2C; exc: WT 1.00 ± 0.03, Bsn^{GT} 1.40 ± 0.04; inh: WT 1.00 ± 0.05, Bsn^{GT} 1.09 ± 0.03). This result indicates increased CDK5-mediated phosphorylation of Ser551 of Syn1 in excitatory but not in inhibitory synapses in Bsn^{GT} mice.

The kinase activity of CDK5 at the presynapse is under the control of neuronal activity (Kim & Ryan, 2010). Bsn deletion leads to epileptic seizures (Altrock *et al*, 2003) and it is, therefore, possible that increased endogenous network activity triggers higher activation of CDK5 in Bsn^{GT}. To address this, we treated both WT and Bsn^{GT} neurons with tetrodotoxin (TTX) and bicuculline (BIC), which decreases or increases, respectively, phosphorylation at Ser551 of Syn1 in cultured neurons (Verstegen *et al*, 2014). In line with published data, TTX treatment (1 μM, 72 h) significantly decreased, while application of BIC (30 μM, 48 h) significantly elevated Ser551Syn1 phosphorylation in WT neurons (Fig 3G and H; WT 1.00 ± 0.05, WT + TTX 0.68 ± 0.03, WT + BIC 1.43 ± 0.11). However, neither of the treatments affected the pSer551Syn1 in Bsn^{GT} neurons (Fig 3G and H; Bsn^{GT} 1.40 ± 0.07, Bsn^{GT} + TTX 1.16 ± 0.06, Bsn^{GT} + BIC 1.36 ± 0.13). These data indicate that increased activity of CDK5 at presynapse contributes to the changes in SV pools in Bsn^{GT} neurons. Moreover, they revealed a failure in neuronal activity-dependent regulation of presynaptic CDK5 activity in the absence of Bsn.

Regulation of RRP by PKA and calcineurin is dysregulated upon Bsn deletion

Calcineurin is the Ser/Thr phosphatase that counteracts the action of CDK5 in the regulation of neurotransmitter release (Fig 3D) (Kim &

Ryan, 2010, 2013). To address the role of calcineurin in the dysregulation of SVs pools in Bsn^{GT} neurons, we applied the calcineurin inhibitor FK506 (1 μM) to neurons 0.5 h prior to imaging of SV pools. This treatment significantly decreased TRP in WT but had no additional effect on Bsn^{GT} neurons, resulting in the same residual TRP in both genotypes (Fig 4A, B, and D; TRP: WT 0.41 ± 0.01, WT + FK506 0.27 ± 0.02, Bsn^{GT} 0.29 ± 0.02, Bsn^{GT} + FK506 0.27 ± 0.02). These data are in line with the role of the CDK5/calcineurin balance in the regulation of TRP in WT and with a shift in this balance towards increased CDK5 activity in Bsn^{GT} neurons (Fig 3C). Interestingly, calcineurin inhibition had no significant effect on the RRP size in WT, but it significantly increased RRP size in Bsn^{GT} neurons and in fact normalised the impairment in RRP size seen in the absence of Bsn (Fig 4A–C; WT 0.11 ± 0.00, WT + FK506 0.09 ± 0.01, Bsn^{GT} 0.08 ± 0.01, Bsn^{GT} + FK506 0.11 ± 0.01). This observation suggests that depending on the presence of Bsn calcineurin differentially regulates the RRP.

PKA is a critical regulator of RRP in chromaffin cells, with Thr138 of SNAP25 (pThr138SNAP25) being the known target of its action in this context (Fig 4G) (Risinger & Bennett, 1999; Nagy *et al*, 2004). Phosphatase activity of calcineurin antagonises this effect of PKA by dephosphorylation of pThr138SNAP25 (Nagy *et al*, 2004). Thus, we compared the phosphorylation of SNAP25 in WT and Bsn^{GT}. Using quantitative immunoblots, we detected significantly lower immunoreactivity for pThr138SNAP25 in the membrane fraction P2 prepared from Bsn^{GT} hippocampal lysates, while the total expression of SNAP25 was unchanged between genotypes (Fig 4E and F; WT 1.00 ± 0.07, Bsn^{GT} 0.53 ± 0.05). Subsequent, direct measurement of enzyme activity showed significantly increased calcineurin phosphatase activity and decreased PKA activity in the hippocampal lysates from Bsn^{GT} (Fig 4H and I; calcineurin: WT 1.00 ± 0.06, Bsn^{GT} 1.42 ± 0.11; PKA: WT 1.00 ± 0.06, Bsn^{GT} 0.73 ± 0.05). Thus, these results indicate that lack of Bsn induces an aberrant presynaptic activity of calcineurin and PKA.

PKA-dependent regulation of SV pools is shifted and insensitive to forskolin in Bsn^{GT}

To test the contribution of PKA in the decreased RRP and TRP size, we compared the effect of pharmacological manipulation of PKA activity on SV recycling visualised by imaging of sypHy fluorescence in WT and Bsn^{GT} neurons. First, we performed measurements in

Figure 3. CDK5-dependent phosphorylation of Ser551 of Syn1 is increased in Bsn^{GT} *in vivo* and *in vitro* and not regulated by neuronal activity *in vitro*.

- A Representative immunoblot with antibody against CDK5-dependent pSer551 of Syn1 (pSer551Syn1) and total Syn1 and total protein stain used as loading control for quantification of Syn1 on P2 fractions prepared from hippocampal tissue lysates of WT and Bsn^{GT} mice.
- B, C Quantification of pSer551Syn1 /Syn1 ratio (in B) and total Syn1 (in C) abundance on blots from (A).
- D Scheme depicts the regulation of phosphorylation of Ser551 of Syn1 by CDK5/calcineurin balance that mediates recruitment of SVs from TRP to the ResP. Changes in this signalling detected in Bsn^{GT} neurons are depicted in red.
- E Representative images of 19 DIV cultured hippocampal neurons from WT and Bsn^{GT} immunostained for pSer551Syn1 and total Syn1.
- F Quantification of IF intensity of pSer551Syn1 in synapses from WT, Bsn^{GT} and WT cells treated with roscovitine.
- G Representative images of 21 DIV hippocampal WT and Bsn^{GT} neurons at baseline activity, upon network activity silencing (TTX, 1 μM, 72 h) or in conditions of increased activity (BIC, 30 μM, 48 h).
- H Quantification of experiment in (G).

Data information: In the plots, the interquartile range and median are depicted as boxes, minimal and maximal values as whiskers and + indicates mean. The sample size *n* (in brackets) corresponds to the number of independently processed animals in (B) and (C) or to the number of independent images (E, G) quantified from two (F) and four (H) independent cultures per condition. For statistics, the Student's *t*-test in (B) and (C) one-way ANOVA with the Sidak's multiple comparison test in (F) and two-way ANOVA with the Tukey's multiple comparison test in (H) were used, **P* ≤ 0.05, ***P* < 0.01, ****P* < 0.001. Scale bar is 5 μm in (E) and (G).

cells of both genotypes treated with H89 (10 μ M, 1 h), a potent inhibitor of PKA. The analysis revealed a significant drop in both RRP and TRP in WT neurons (Fig 5A–D; RRP: WT 0.13 ± 0.01 , WT + H89 0.08 ± 0.01 ; and TRP: WT 0.40 ± 0.01 , WT + H89

0.29 ± 0.03). This is in line with a requirement for PKA activity in the regulation of RRP and TRP. The same treatment had a minor effect on RRP and TRP in Bsn^{GT}, indicating very low PKA activity in the absence of Bsn (Fig 5A–D; RRP: Bsn^{GT} 0.09 ± 0.01 ,

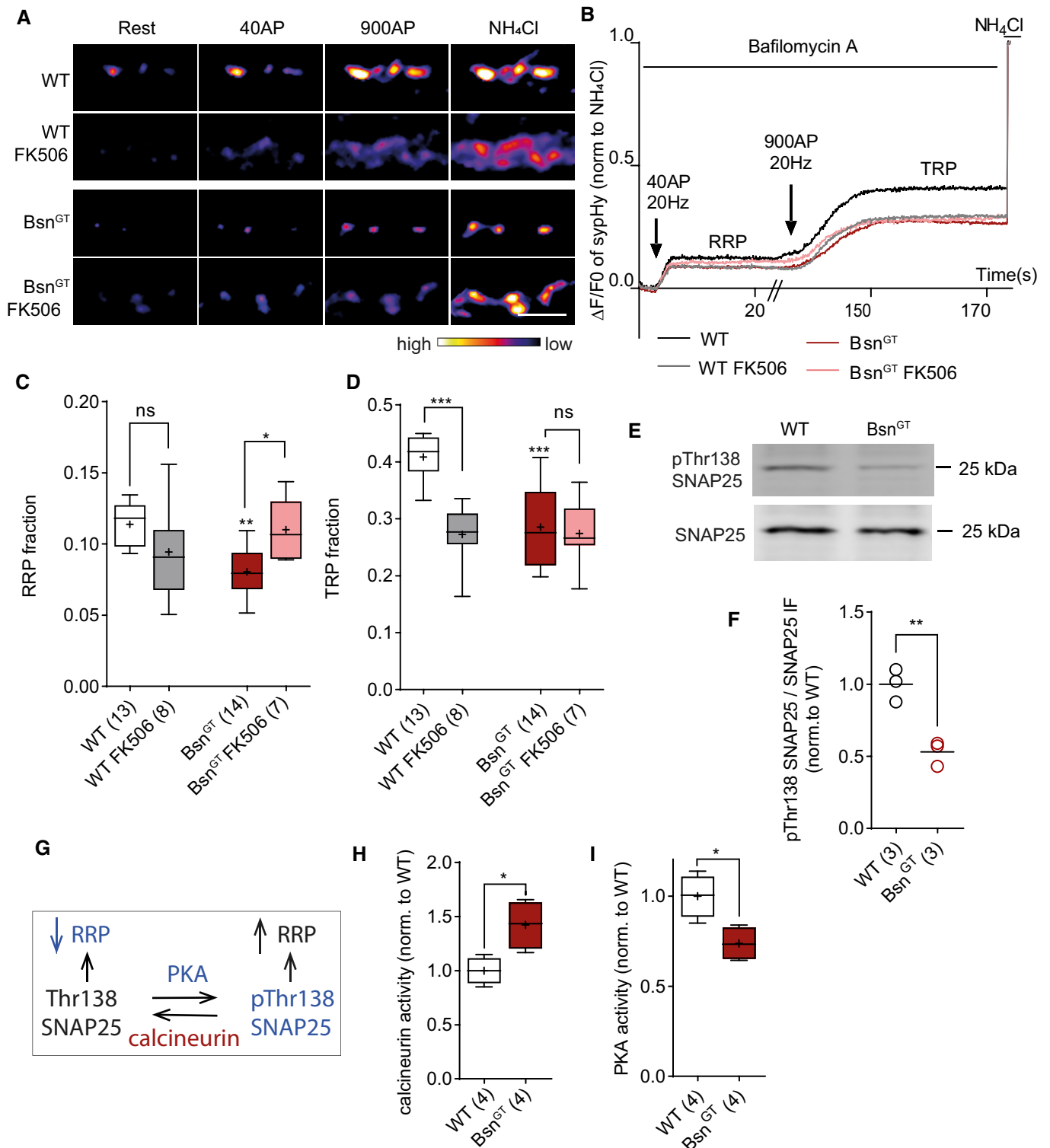


Figure 4.

Figure 4. Decreased PKA and increased calcineurin activity in Bsn^{GT} neurons.

- A, B Representative pseudo colour images (A) and average traces (B) of sypHy fluorescence plotted from WT and Bsn^{GT} hippocampal neurons treated with calcineurin inhibitor FK506.
- C, D Quantification of the RRP and TRP fractions in WT and Bsn^{GT} neurons from the experiment in (A) and (B).
- E Representative Western blot on P2 fractions prepared from hippocampal tissue of WT and Bsn^{GT} mice probed with antibodies against SNAP25 phosphorylated on Thr138 and total SNAP25.
- F Quantification of blot in (E) shows lower pThr138SNAP25 to total SNAP25 IF ratio in Bsn^{GT} compared with WT.
- G Scheme illustrates the PKA/calcineurin-dependent regulation of SNAP25 phosphorylation on its Thr138 that promotes enlargement of RRP via an increase in SV release competence. The changes detected in Bsn^{GT} are depicted in red for elevated and in blue for lowered abundance/activity.
- H, I Direct activity measurements reveal a significant increase in calcineurin and a drop in PKA activity in samples prepared from hippocampal tissue of Bsn^{GT} mice as compared with their WT littermates.

Data information: In all plots, the interquartile range and median are depicted as boxes, minimal and maximal values as whiskers, and + indicates mean. The sample size is given in brackets for each quantification and reflects the number of analysed imaging experiments done on three independently prepared cultures per genotype in (B–D) and the number of animals per genotype used for WB or enzyme activity measurements in (F), (H) and (I). Statistical significance was assessed using two-way ANOVA with the Tukey's multiple comparison test for (C) and (D) and the Student's *t*-test in (F), (H) and (I); significance is depicted as follows: **P* ≤ 0.05, ***P* < 0.01, ****P* < 0.001. Scale bar is 2 μm.

Bsn^{GT} + H89 0.07 ± 0.01 and TRP: Bsn^{GT} 0.29 ± 0.02, Bsn^{GT} + H89 0.27 ± 0.01). Next, we applied forskolin (50 μM, 1 h), a potent nonselective activator of adenylyl cyclases (ACs). ACs are the enzymes catalysing the conversion of ATP to cAMP and are therefore upstream of PKA activation. In line with the central role of PKA in the regulation of RRP and TRP, forskolin application induced a significant increase in RRP and TRP in WT neurons. Strikingly, forskolin application had no effect on RRP and TRP in the Bsn^{GT} neurons, indicating a defect in forskolin-induced AC activation in the absence of Bsn (Fig 5A–D; RRP: WT + forskolin 0.17 ± 0.01; Bsn^{GT} + forskolin 0.10 ± 0.01; TRP: WT + forskolin 0.50 ± 0.01, Bsn^{GT} + forskolin 0.32 ± 0.03).

The regulation of RRP and TRP by PKA relies largely on PKA-dependent phosphorylation of Ser9 of Syn1 (pSer9Syn1), which regulates the association of SV with actin filaments and their recruitment to the release sites (Fig 5J) (Menegon *et al*, 2006; Valente *et al*, 2012). Ser9 of Syn1 is also a target of Calmodulin kinase I and IV (Huttner *et al*, 1981). To isolate the PKA-dependent pSer9Syn1, we performed all the immunoblots and immunolabelling experiments in the presence of CaMK inhibitor KN93 (4 μM) as described earlier (Menegon *et al*, 2006). In line with the decreased presynaptic PKA activity in Bsn^{GT} neurons, the phosphorylation of pSer9Syn1/Syn1 ratio was significantly decreased in the P2 membrane fraction of hippocampal lysates from Bsn^{GT} mice compared with WT (Fig 5E and F; WT 1.00 ± 0.10, Bsn^{GT} 0.40 ± 0.02). Interestingly, the total

immunoreactivity of Syn1 in this fraction was significantly elevated in Bsn^{GT} than in WT samples indicating a higher membrane association of Syn1 in the absence of Bsn under this condition (Fig 5E and G; WT 1.00 ± 0.14, Bsn^{GT} 1.31 ± 0.16). Analyses of immunoreactivity for pSer9Syn1 in individual synapses further confirmed that phosphorylation of this critical residue correlates with the functional impairment of RRP and TRP in Bsn^{GT} neurons. Specifically, the pSer9Syn1 immunoreactivity was significantly lower in Bsn^{GT} neurons under basal conditions (Fig 5H and I; WT 1.00 ± 0.04, Bsn^{GT} 0.70 ± 0.05) and the treatment with H89 decreased pSer9Syn1 immunoreactivity in WT neurons to the levels measured in Bsn^{GT} (Fig 5H and I; WT + H89 0.67 ± 0.08, Bsn^{GT} + H89 0.61 ± 0.02). Application of forskolin resulted in increased pSer9Syn1 immunoreactivity in WT neurons but had no significant effect in Bsn^{GT} (Fig 5I and J; WT+ forskolin 1.31 ± 0.04, Bsn^{GT} + forskolin 0.81 ± 0.06). In the next step, we analysed immunoreactivity for total Syn1 and for pSer9Syn1 in individual excitatory and inhibitory synapses labelled with VGLUT1 and VGAT antibodies, respectively (Fig 5V3A). The analyses revealed that while the immunoreactivity for Syn1 was unchanged between WT and Bsn^{GT} in both synapse types, the labelling for pSer9Syn1 (relative to IF of total Syn1 at the same synapse) was significantly reduced in Bsn^{GT} excitatory but not in inhibitory synapses (Fig 5V3B and C; exc: WT 1.00 ± 0.05, Bsn^{GT} 0.68 ± 0.04; inh: WT 1.00 ± 0.08, Bsn^{GT} 0.88 ± 0.06). Collectively, these data indicate that dysregulation of PKA activity that

Figure 5. PKA-dependent phosphorylation of Syn1 is decreased and insensitive to forskolin in Bsn^{GT}.

- A, B Representative pseudo colour images (A) and average traces (B) of sypHy fluorescence plotted for WT and Bsn^{GT} neurons without treatment (black and red) and upon treatment with adenylyl cyclase activator forskolin (grey and pink) or PKA inhibitor H89 (light grey and orange).
- C, D Quantification of the RRP and TRP fraction from the experiment in (A) and (B).
- E Representative immunoblot with antibody against pSer9Syn1 and total Syn1 and total protein stain of hippocampal P2 fraction from WT and Bsn^{GT} mice prepared in the presence of KN93 to isolate PKA-dependent regulation of pSer9Syn1.
- F, G Quantification of pSer9Syn1/Syn1 ratio (in F) and Syn1 (in G) on blots from (E).
- H Representative images of hippocampal neurons from WT and Bsn^{GT} mice labelled with antibodies against pSer9Syn1 and total Syn1. Neurons were pretreated (4 μM, 1 h) with KN93 to isolate PKA-dependent phosphorylation and then treated in addition with forskolin or H89 before fixation.
- I Quantification of staining in (H).
- J Scheme illustrates the PKA-dependent phosphorylation of Syn1 on Ser9 that promotes recruitment of SVs to the recycling pool. Changes in this signalling confirmed in Bsn^{GT} are depicted in red.

Data information: In the plots, the interquartile range and median are depicted as boxes, minimal and maximal values as whiskers, and + indicates mean. The sample size is given in brackets and corresponds to the number of analysed independent imaging experiments performed on three independently prepared culture batches in (C and D), samples prepared from individual animals in (F) and (G), or quantified independent visual fields obtained from two independent culture preparations in (I). The statistical significance was assessed in (C), (D) and (I) using two-way ANOVA with the Tukey's multiple comparison test and in (F) and (G) using the Student's *t*-test as is depicted in graphs as **P* ≤ 0.05, ***P* < 0.01, ****P* < 0.001. The scale bar is 2 μm in (A) and 5 μm in (H).

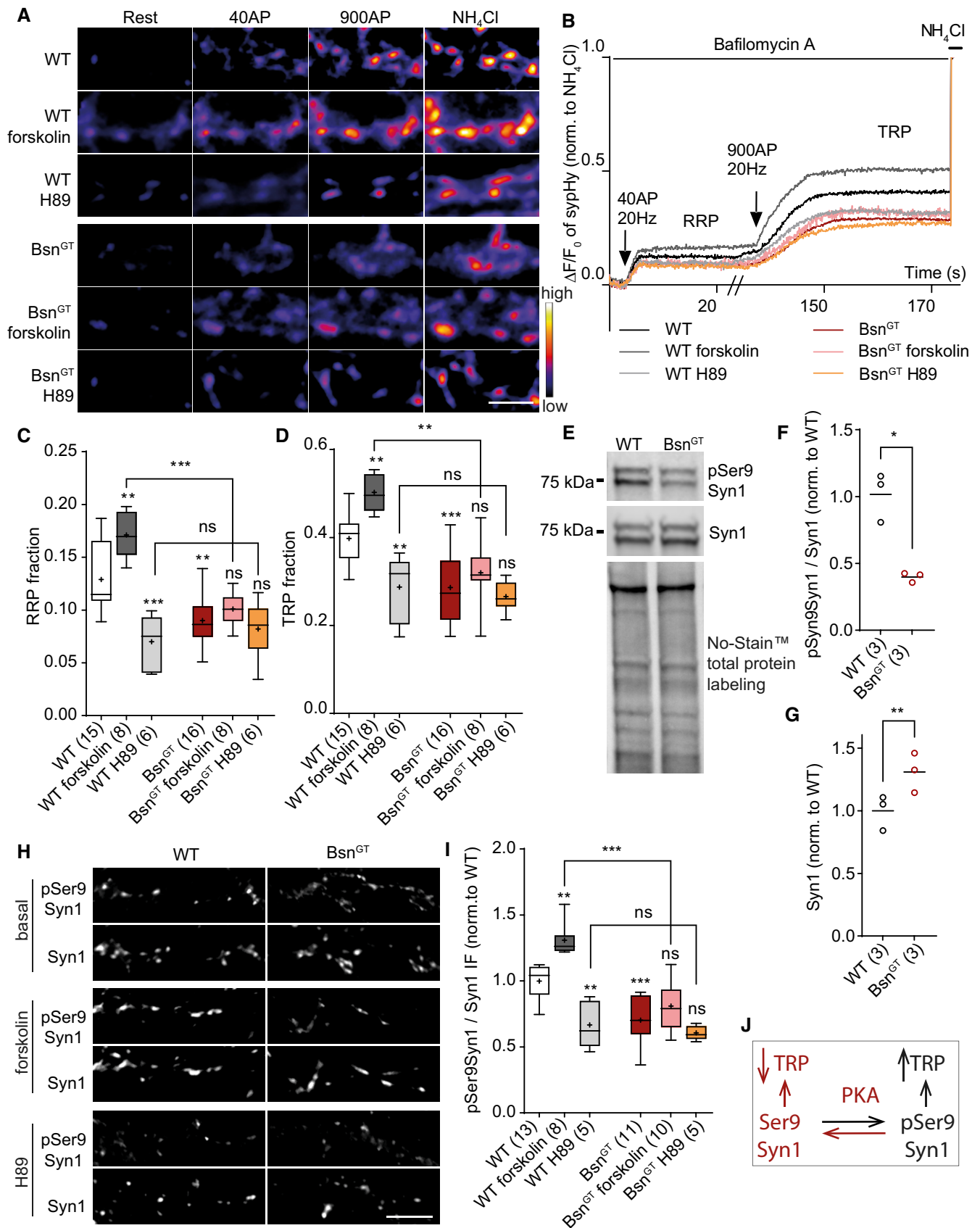


Figure 5.

acts, amongst others, via phosphorylation Ser⁹ of Syn1 underlies the decrease in RRP and TRP in Bsn^{GT} excitatory synapses. Moreover, since the application of AC activator forskolin cannot normalise the dysregulation of SV pools in Bsn^{GT}, they indicate an uncoupling of AC-cAMP-PKA signalling in the absence of Bsn.

PDE4 controls SV pools and is dysregulated in Bsn^{GT}

The failure of forskolin to potentiate SV recycling in Bsn^{GT} might be due to the loss of PKA responsiveness to cAMP or due to an aberrant cAMP metabolism. To address this, we utilised an analogue of cAMP, Sp-isomer of N6-Benzoyladenine-3',5'-cyclic monophosphorothioate (6-Bnz-cAMPS) that acts as a specific activator of PKA and is resistant to hydrolysis by phosphodiesterases (PDEs). We treated cultured WT and Bsn^{GT} neurons with 6-Bnz-cAMPS (50 μ M, 1 h) and analysed the effect of this treatment on SV recycling (Fig 6A and B). The treatment increased RRP by 42% and TRP by 31% in WT but had a significantly larger effect on Bsn^{GT} neurons, increasing RRP by 78% and TRP by 56% (Fig 6E). Importantly, the application of 6-Bnz-cAMPS completely normalised the differences in SV pools measured in untreated Bsn^{GT} neurons (Fig 6A–D; RRP: WT 0.12 \pm 0.01, WT + 6-Bnz-cAMPS 0.17 \pm 0.01, Bsn^{GT} 0.08 \pm 0.01, Bsn^{GT} + 6-Bnz-cAMPS 0.15 \pm 0.01 and TRP: WT 0.38 \pm 0.02, WT + 6-Bnz-cAMPS 0.50 \pm 0.03, Bsn^{GT} 0.29 \pm 0.01, Bsn^{GT} + 6-Bnz-cAMPS 0.45 \pm 0.03). Thus, the decreased release and recycling competence of SV in Bsn^{GT} is likely due to the lower cAMP abundance in the absence of Bsn. Indeed, a direct measurement revealed lower cAMP concentration in the hippocampal tissue of Bsn^{GT} mice compared with their WT littermates (Fig 6F; WT 1.00 \pm 0.02, Bsn^{GT} 0.78 \pm 0.03).

cAMP signalling is terminated by hydrolysis of cAMP by enzymes phosphodiesterases, with PDE4 isoform being the most abundant enzyme isoform in the brain. To address a possible role of PDE4 in the regulation of SV recycling, we applied the PDE4 inhibitor rolipram (1 μ M, 0.5 h) to neurons of both genotypes. This treatment led to an increase in RRP by 39% and TRP by 29% in WT but had again much stronger effect in Bsn^{GT}, where it increased the RRP by 78% and TRP by 56% (Fig 6E). Importantly, similar to 6-Bnz-cAMPS, rolipram treatment fully masked the differences in SV pools between the genotypes (Fig 6A–E; RRP: WT + rolipram 0.16 \pm 0.01, Bsn^{GT} + rolipram 0.14 \pm 0.01, TRP: WT + rolipram 0.49 \pm 0.02, Bsn^{GT} + rolipram 0.44 \pm 0.02). These results indicate that increased PDE4-dependent hydrolysis of cAMP underlies the

differences in SV recycling in the absence of Bsn. In support of this conclusion, we detected significantly higher PDE4-associated phosphodiesterase activity in the hippocampal tissue of Bsn^{GT} mice compared with their WT littermates (Fig 6G; WT 1.00 \pm 0.07, Bsn^{GT} 1.46 \pm 0.05).

PKA-dependent phosphorylation of the upstream conserved region 1 (UCR1) of PDE4 is a well-established regulatory mechanism that increases the activity of long PDE4 isoforms (MacKenzie *et al*, 2002). Therefore, it was surprising to detect high PDE4 activity in the condition of low PKA phosphorylation in Bsn^{GT}. Recently, a new CDK5-dependent regulation of PDE4 activity was discovered in neurons. Specifically, CDK5 phosphorylation at Ser145 within the UCR1 (pSer145PDE4B) significantly increased PDE4 phosphodiesterase activity also in the absence of PKA activation (Plattner *et al*, 2015). Our data indicated an increased presynaptic CDK5 activity in Bsn^{GT} (Fig 3A–E). To test the possible CDK5-dependent activation of PDE4 in Bsn^{GT} we quantified phosphorylation of the CDK5-dependent phosphorylation site in PDE4 (pSer145 PDE4B) in WT and Bsn^{GT} hippocampal homogenates using a phosphospecific antibody (Plattner *et al*, 2015). We detected significantly higher levels of CDK5-dependent PDE4B phosphorylation in Bsn^{GT}, indicating that activation of PDE4 by its CDK5-dependent phosphorylation drives the exacerbated cAMP hydrolysis observed upon deletion of Bsn (Fig 6H and I; WT 1.00 \pm 0.11 vs. Bsn^{GT} 1.92 \pm 0.29). Together, these data confirm that reduction in the fraction of releasable SVs in the absence of Bassoon relies on depletion of cAMP due to dysregulation of its PDE4-dependent hydrolysis downstream of CDK5 (Fig 6J). Moreover, they also reveal a new role of CDK5-PDE4-cAMP-PKA signalling axis in the regulation of presynaptic release competence.

Discussion

Imaging of SV pools in Bsn^{GT} reveal a decrease in SV release competence in excitatory synapses

Despite the well-documented impact of Bsn deletion on synaptic neurotransmission, the molecular understanding of this impairment remained limited. In this work, we explored the effect of genetic ablation of Bsn expression on the recycling and release competence of SVs and dissected the cellular signalling involved in this process. We observed a higher fraction of silent excitatory presynapses in

Figure 6. PDE4 activity inhibition rescues Bsn^{GT} phenotype.

- A, B Representative pseudo colour images (A) and average traces (B) of sypHy fluorescence plotted for untreated WT and Bsn^{GT} neurons (black and red) and cultures treated with 6-Bnz-cAMPS (50 μ M, 1 h; grey and pink) and rolipram (1 μ M, 30 min, light grey and orange).
- C, D Quantifications of RRP and TRP fractions in the experiment in (A) and (B).
- E Effect of treatment is significantly higher in Bsn^{GT} than in WT.
- F, G Quantification of cAMP levels and PDE4-associated phosphodiesterase activity assessed in hippocampal tissue of WT and Bsn^{GT} animals.
- H Quantification of pSer145PDE4B to the total PDE4B ratio from the experiment in (I).
- I Representative immunoblot with antibody against CDK5-dependent pSer145PDE4B and total PDE4B on hippocampal tissue from WT and Bsn^{GT} animals.
- J The scheme illustrates the CDK5-dependent regulation of cAMP hydrolysis by PDE4 and the downstream effect of PKA affecting the TRP size. The changes in this signalling detected in Bsn^{GT} are shown; blue indicates decreased and red an increased activity or abundance.

Data information: In the plots, the interquartile range and median are depicted as boxes, minimal and maximal values as whiskers, and + indicates mean. The sample size is given in brackets and corresponds to the number of imaging experiments performed on three independently prepared cultures in (C–E) or individual animals used for sample preparation in (F–H). Statistical significance was assessed using two-way ANOVA with the Tukey's multiple comparison test in (C), (D) and (E) and the Student's *t*-test in (F), (G) and (H) and is given as: **P* \leq 0.05, ***P* < 0.01, ****P* < 0.001. Scale bar is 2 μ m.

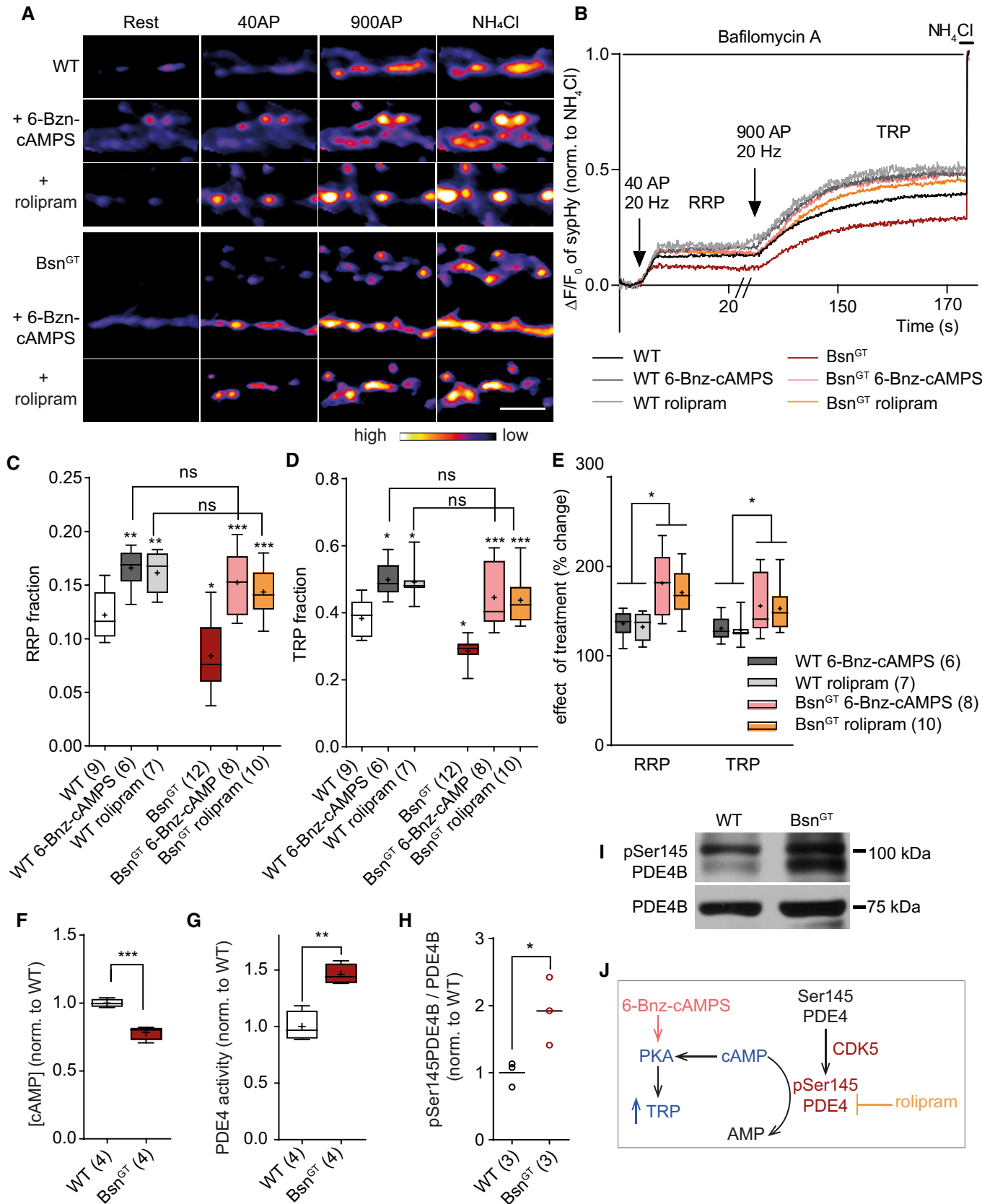


Figure 6.

Bsn^{GT} cultured neurons compared with WT, which is reminiscent of data obtained by early analyses of mutant mice lacking the central region of the Bsn protein (Altrock *et al*, 2003). This previous study reported functional inactivation of a fraction of synapses leaving the remaining synapses unaffected and postulated that a subset of synapses relies on normal Bsn expression (Altrock *et al*, 2003). Our current data modify this statement revealing Bsn as a universally acting factor necessary for proper release competence in glutamatergic synapses. We observed reduced sizes of RRP and TRP of SVs evoked by electrical and chemical stimulation. Reduced RRP has been detected by electrophysiological measurements in glutamatergic synapses of cultured hippocampal neurons, endbulb of Held and ribbon synapses of inner ear cells (IHC), and cone photoreceptors in Bsn mutants (Altrock *et al*, 2003; Buran *et al*, 2010; Frank *et al*, 2010; Jing *et al*, 2013; Mendoza Schulz *et al*, 2014; Babai *et al*, 2019, 2021). In synapses with the high-frequency release, such as cerebellar mossy fibre to granular cell synapse, IHC ribbon synapse and cone photoreceptors, the deletion of Bsn led to the more pronounced depression of neurotransmission upon repetitive stimulations (Frank *et al*, 2010; Hallermann *et al*, 2010; Jing *et al*, 2013; Babai *et al*, 2019, 2021). The stronger depression of neurotransmission was attributed to a slower replenishment of SVs, which is well compatible with a smaller total recycling pool of SVs shown in this study. Thus, the data obtained using the imaging approach in cultured neurons in this study are in good accordance with the previously published data generated by alternative methodologies and using *ex vivo* preparations.

Aberrant SV recycling relies on defects in presynaptic phospho-homeostasis upon Bsn loss

Our experiments could confirm previously described effect of Bsn loss on the synaptic abundance of other presynaptic proteins important for SV release such as Munc13-1 and Pclo. However, this effect was similar in excitatory and inhibitory synapses, which argues against a causal relationship of these changes with decreased release competence of SVs observed upon Bsn deletion, specifically in excitatory synapses. In contrast, changes in the phosphorylation levels of Ser9 and Ser551 of Syn1 were detectable in excitatory but not in inhibitory synapses in Bsn^{GT} neurons, strongly supporting our notion that changes in synaptic phosphorylation underlie the decline in SV release competence observed in glutamatergic synapses lacking Bsn expression. Our experiments conclude that Bsn is crucial for the maintenance of normal dynamic phosphorylation at presynapse (Fig 7). We measured lower PKA catalytic activity and detected lower phosphorylation of known presynaptic substrates of PKA in the absence of Bsn *in vivo* and *in vitro*. The decreased PKA activity was a consequence of dysregulation in the metabolism of cAMP due to its increased hydrolysis and inefficient production. cAMP and its downstream target PKA are the major regulators of presynaptic plasticity (Huang *et al*, 1994). PKA activation has been linked to the increase in vesicular release probability but also to an increment in SV release competence and RRP size, which were reduced in Bsn^{GT} mice as shown in previous studies and in this work (Chen & Regehr, 1997; Lonart *et al*, 1998; Menegon *et al*, 2006; Moulder *et al*, 2008; Vaden *et al*, 2019). cAMP signalling plays a major role in the regulation of SVs at the glutamatergic synapse by neuromodulators (Patzke *et al*, 2019, 2021). Therefore, it will be interesting

to investigate the effect of Bsn deletion on neuromodulation in future studies. Our experiments also revealed enhanced CDK5-dependent phosphorylation of synaptic targets in Bsn^{GT} neurons. CDK5 regulates the release competence of SVs and drives their assignment to the ResP (Kim & Ryan, 2010, 2013; Verstegen *et al*, 2014). In line with the increased CDK5 activity, we observed increased ResP in the absence of Bsn. Acute pharmacological activation of PKA or inhibition of CDK5 fully normalised the defect in SV recycling in the absence of Bsn, confirming the pivotal role of the aberrant activity of these enzymes in the decline of SV release competence in Bsn^{GT} neurons. The acute rescue of Bsn^{GT} phenotype also confirms that aberrant presynaptic signalling and not structural or developmental impairments cause the defects in SV recycling in the absence of Bsn. Finally, our experiments revealed a dual role of phosphatase calcineurin in the regulation of SV recycling. Calcineurin antagonises the effect of CDK5 on the recruitment of SVs into the ResP (Kim & Ryan, 2010, 2013). Compliant with this, calcineurin inhibition decreased the TRP in WT neurons and fully phenocopied the Bsn^{GT} situation indicating that acute shift of CDK5/calcineurin balance in favour of CDK5 induced a fast decrease in release competence of SVs and their assignment to the ResP. Unexpectedly, calcineurin inhibition in Bsn^{GT} but not in WT increased RRP. Calcineurin antagonises PKA-dependent phosphorylation of Thr138 of SNAP25, which is required for the maintenance of RRP in chromaffin cells (Nagy *et al*, 2004). The selective effect of calcineurin inhibition on RRP in Bsn^{GT} is therefore consistent with elevated calcineurin and with decreased PKA activity that we observed in the absence of Bsn and indicates a role of calcineurin by antagonising PKA in the regulation of RRP in glutamatergic synapses (Fig 4G).

PDE4 regulates SV pools

Unexpectedly, acute pharmacological inhibition of CDK5, which is known to promote the recruitment of SVs to ResP, also affected the size of RRP in both WT and Bsn^{GT} neurons. We sought a possible explanation and realised that CDK5 was linked to the regulation of cellular cAMP signalling in the forebrain (Guan *et al*, 2011; Plattner *et al*, 2015). Specifically, the phosphorylation by CDK5 was demonstrated to stimulate the phosphodiesterase activity of PDE4, decreasing the cAMP levels, which attenuates the kinase activity of PKA (Plattner *et al*, 2015). In Aplysia, it was shown that presynaptic PDE4 controls the PKA activity and synaptic facilitation (Park *et al*, 2005). However, the role of PDE4-dependent hydrolysis of cAMP in the regulation of neurotransmitter release in vertebrate neurons remained elusive. We detected increased CDK5-dependent phosphorylation of PDE4 and enhanced hydrolytic activity of PDE4 in Bsn^{GT}. Inhibition of PDE4 activity by rolipram or application of cAMP analogue resistant to PDE4-dependent hydrolysis fully normalised the SV pools in Bsn^{GT} neurons. Thus, we demonstrated that dysregulation of SV pools in the absence of Bsn results from profound dysregulation of presynaptic cAMP signalling. Our data also revealed a new role for PDE4 in the crosstalk of CDK5/calcineurin and cAMP/PKA-dependent regulation of SV recycling and reveal a dual role of presynaptic CDK5 activity that directly reduces SV availability for release by their shift to ResP and indirectly by decreasing RRP via PDE4-mediated inhibition of cAMP signalling. PDE4 has been linked to the pathophysiology of schizophrenia. The product

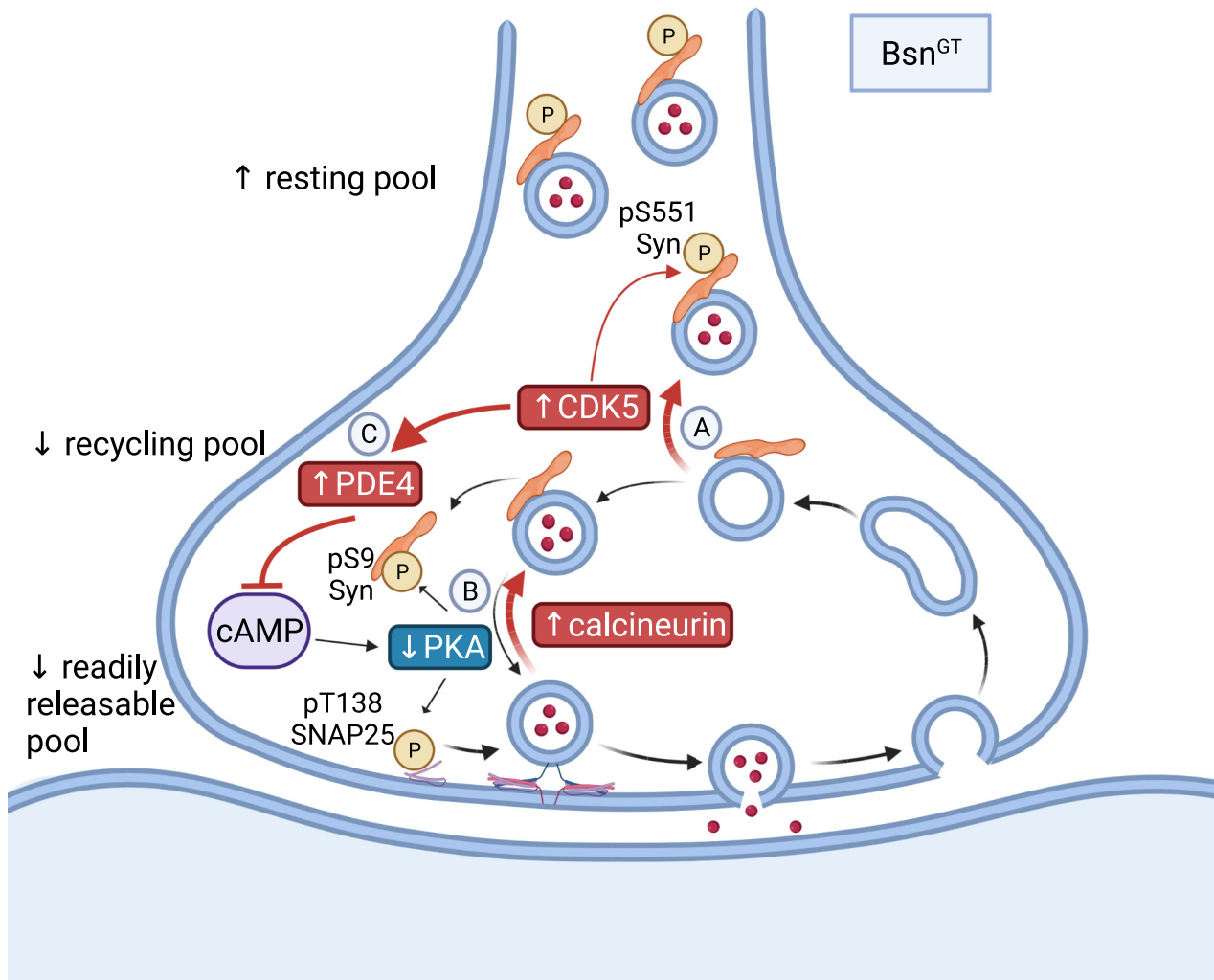


Figure 7. Graphical summary.

The scheme summarises the dysregulation of CDK5/PDE4/cAMP/PKA axis and aberrant phosphorylation of SNAP25 and synapsin in the absence of Bsn. Bsn deletion induces (A) dysregulation of CDK5 and (B) PKA/calcineurin balance leading to changes in the phosphorylation levels of effector proteins SNAP25 and synapsin. The aberrant signalling causes the functional defects, namely, a decline in release competence and an increased proportion of release-unable vesicles observed in neurons with Bsn deletion. Moreover, as depicted in (C) this work reveals regulation of PDE4 by CDK5 upstream of cAMP/PKA-dependent control of SV release competence. Illustration was prepared using BioRender.com.

of a schizophrenia risk gene, DISC1, binds and regulates PDE4 activity, which is dysregulated in psychotic patients and animal models (Millar *et al*, 2005). Application of selective PDE4 inhibitor rolipram rescued impaired LTP and behavioural deficits in pharmacologically and genetically-induced animal model of psychosis by presynaptic mechanisms indicating a role of PDE4 in presynaptic plasticity (Wiescholleck & Manahan-Vaughan, 2012; Kim *et al*, 2021). Our work now directly demonstrates an effect of PDE4 on the regulation of SV release competence and thus provides a cellular substrate for the PDE4-dependent modulation of presynaptic plasticity.

How can Bsn connect to the regulation of dynamic phosphorylation at presynapse?

We have shown previously that Bsn organises presynaptic voltage-gated calcium channels in neuronal cell types (Frank *et al*, 2010;

Hallermann *et al*, 2010; Ryl *et al*, 2021). In cortical and hippocampal synapses, it is required for specific recruitment of Cav2.1 (P/Q-type channels) channels to the release sites and consequently, relatively more Cav2.2 (N-type) channels are present at synapses in the absence of Bsn (Davydova *et al*, 2014). Interestingly, previous studies linked the Cav2.2 to the activity-dependent regulation of presynaptic CDK5/calcineurin activities (Su *et al*, 2012; Kim & Ryan, 2013). Future studies will be necessary to address whether the dysregulation of presynaptic phosphorylation in Bsn^{GT} originates from aberrant presynaptic calcium influx in the absence of Bsn. Another possible explanation of the effect of Bsn deletion on presynaptic phosphorylation status described in this work is the potential role of Bsn in the scaffolding of presynaptic kinase/phosphatase signalling complexes. The kinase scaffolding proteins such as 14-3-3s or AKAPs emerged to increase the selectivity and efficiency of substrate recognition and recruitment (Fu *et al*, 2000;

Torres-Quesada *et al*, 2017). Indeed, Bsn interacts with 14-3-3s, which can recruit signalling complexes to the active zone (Schroder *et al*, 2013). Moreover, Bsn emerged as a heavily phosphorylated protein and several studies revealed significant changes in its phosphorylation pattern during neuronal activity (Kohansal-Nodehi *et al*, 2016; Engholm-Keller *et al*, 2019; Silbern *et al*, 2021). Thus, Bsn might act as a docking site for multiple signalling complexes at presynapse and organise the neuronal activity-dependent presynaptic signalling. Future work will be necessary to explore the individual molecular interactions behind the Bsn-linked regulation of presynaptic kinase/phosphatase dynamics.

Previous publications highlighted the role of Bsn in the regulation of presynaptic ubiquitination, proteasomal activity and autophagy (Waites *et al*, 2013; Hoffmann-Conaway *et al*, 2020; Montenegro-Venegas *et al*, 2021). Moreover, aberrant ubiquitination of SV proteins and enhanced degradation of entire SVs via autophagy and endo-lysosomal pathway was observed in cultured Bsn^{GT} neurons (Hoffmann-Conaway *et al*, 2020). It has been proposed that “old” SVs putatively containing misfolded proteins contribute less efficiently to the neurotransmission and locate more preferentially to the resting pool (Truckenbrodt *et al*, 2018). Thus, changes in the release competence of SVs and their distribution to the pools can be causally connected to an aberrant turnover of SV proteins in absence of Bsn. Up to date, it is incompletely understood how cellular signalling controls ubiquitination and endo-lysosomal pathway. In this work, we demonstrated that acute pharmacological interference with dysregulated signalling completely rescued the release competence of SVs in absence of Bsn. It will be interesting to investigate, whether the same signalling networks also control the turnover of SV proteins.

Materials and Methods

Animals

Bassoon gene-trap mice (Bsn^{Gt(OST486029)Lex}, MGI:4880009) were generated from Omnibank ES cell line OST486029 by Lexicon Pharmaceuticals, Inc. (The Woodlands, TX) as reported previously (Hallermann *et al*, 2010). To get the respective Bsn^{GT} and WT animals for our studies, heterozygous animals were backcrossed for 8–10 generations to C57BL/6N background and then bred in a 2:1 ratio. Animals were bred and housed in groups of 2–5 animals under controlled pathogen-free status with *ad libitum* access to water and standard chow. For primary neuronal culture preparations and all other experiments, animals of both sexes were used.

Ethics approval for experiments using animal material

Breeding of animals and experiments using animal material was carried out in accordance with the European Communities Council Directive (2010/63/EU) and approved by the local animal care committees of Sachsen-Anhalt (Licence number 42502-2-1484 LIN) and of Lower Franconia, Germany (55.2.2-2532-2-1312).

Antibodies

The primary antibodies were used for immunocytochemistry (ICC), Western Blot (WB) and Syt1Ab uptake in the concentration

indicated as follows: rabbit antibodies against Syt1 (labelled with Oyster 550; live staining: 1:70, # 105103C3, Synaptic System, Göttingen, Germany), pThr138SNAP25 (WB:1:500, # 042077, Biomol), SNAP-25 (WB: 1:1,000, # 111002, Synaptic System), pSer9Syn1 (ICC:1:1,000, gift from Dr. Fabio Benfenati, IIT, Genova, Italy), pSer551Syn1 (ICC: 1:1,000, gift from Dr. Anna Fassio, IIT, Genova, Italy), pSer9Syn1 (WB: 1:500, # 2311S, Cell Signalling), pSyn1S553 (human pS553 corresponds to pS551 in mouse;WB: 1:1,000, #ab32532, Abcam), PKA α cat (C-20) (IP 1-2ug, # sc-903, Santa Cruz), PDE4B (H-56) (IP 1-2ug, #sc-25,812, Santa Cruz), pSer145PDE4B (WB 1:200, Plattner *et al*, 2015), Piccolo rb2 44a (ICC: 1:500, LIN Magdeburg), Munc13-1 (ICC: 1:1,000, Synaptic System, # 126103), mouse antibodies against Syn1 (ICC: 1:1,000, WB: 1:1,000, # 106011, Synaptic System), VGLUT1 (ICC:1:1,000, # MAB5502, Millipore), guinea pig antibodies against Syn1 (ICC: 1:1,000, # 106104, Synaptic System), VGAT (ICC:1:1,000, # 131004, Synaptic System), VGLUT1 (ICC:1:1,000, # 135304, Synaptic System) and sheep antibody against PDE4B (WB 1:500, Huston *et al*, 1997). Secondary antibodies used for ICC were: donkey anti mouse coupled with Alexa 488- (ICC 1:2,000, # A21202, Thermo Fisher Scientific), Cy3-donkey anti-rabbit (1:2,000, #711-165-152, Dianova/Jackson ImmunoResearch Labs) and Cy5-donkey anti guinea pig (1:1,000, # 706-175-148, Dianova/Jackson ImmunoResearch Labs). For fluorescent detection of WB, IRDye 680 donkey anti mouse # 926-68072, IRDye 800CW donkey anti guinea pig # 926-32411 and IRDye 680RD donkey anti-rabbit # 926-68071 and secondary antibodies from Li-COR were used. For chemiluminescent detection, Thermo Fisher #31460 anti-rabbit; #A16047 anti-sheep HRP conjugated antibodies were used.

Chemical reagents

D-(-)-2-amino-5-phosphonopentanoic acid (APV) (CAS #79055-68-8), 6-cyano-7-nitroquinoxaline-2,3-dione disodium (CNQX) (CAS #479347-85-8), KN-93 (CAS #139298-40-1), (R)-(-)- Rolipram (CAS # 85416-75-7), TTX (CAS #4368-28-9) and (+)- Bicuculline (CAS #485-49-4) were purchased from Tocris. H-89 (CAS #130964-39-5). Forskolin (CAS #66575-29-9) and FK-506 monohydrat (CAS #109581-93-3), were from Sigma-Aldrich. InSolution Roscovitine (CAS # 186692-46-6) and Bafilomycin A1 (CAS #88899-55-2) were from Calbiochem. N6-Benzoyladeniosine- 3', 5'- cyclic monophosphorothioate, Sp- isomer (Sp-6-Bnz-cAMPS) and sodium salt was from Biolog (CAS # 152218-18-3). The use of limited amounts of TTX, as done in this study, is not subject to special regulations in Germany.

Cultures of primary hippocampal neurons

Primary hippocampal cultures from neonatal (P0-P1) Bsn^{GT} and their WT littermates were prepared as described previously (Altmüller *et al*, 2017; Montenegro-Venegas *et al*, 2021). Briefly, hippocampal tissue was treated with 0.25% (final c) of trypsin (#15090046), and cell suspension was obtained by mechanical trituration. Cells were plated in densities of 35,000 cells per coverslip (18 mm diameter) on poly-L-lysine coated coverslips. One hour after plating, coverslips were transferred with neurons facing down into dishes containing 60–70% confluent monolayer of astrocytes and Neurobasal A medium (#12349015) supplemented with 2%

(v/v) B27 (#17504044), 1 mM sodium pyruvate (#11360070), 4 mM GlutaMAX™ supplement (# 35050038) and antibiotics (100 U/ml penicillin, 100 µg/ml streptomycin, #15240096). About 1 mm large paraffin dots were placed onto coverslips prior to coating and cell plating to assure medium exchange between the feeder layer and neurons during all times of culturing. All chemicals used for neuronal cultures were obtained from Thermo Fisher Scientific unless indicated otherwise. To prevent overgrowth of astroglia 0.6 µM AraC (CAS # 147-94-4, Sigma-Aldrich) was added to the cells on days 1 and 3 after plating to reach a final concentration of 1.2 µM. All cells were maintained at 37°C in a humidified incubator containing 5% CO₂.

Quantitative immunostaining and image analysis

Quantitative immunostainings were performed, acquired and analysed as described previously with minor differences (Lazarevic et al, 2011). For staining, samples compared in one experiment were numbered for blinding and processed in parallel with identical solutions. Image acquisition was done for all samples from one experiment on the same day with identical camera and illumination settings. For IF quantification, 7–12 visual fields from two independent coverslips were acquired and quantified for each experiment in order to reduce experimental variance. Software routines were employed to minimise subjective bias as follows. An unspecific background signal was removed using threshold subtraction in ImageJ software (NIH, <http://rsb.info.nih.gov/ij/>). In all experiments, synaptic puncta were defined semiautomatically by setting rectangular regions of interest (ROI) with dimensions of about 0.8 × 0.8 µm around local intensity maxima in the image with staining for synaptic marker Syn1, VGLUT1 or VGAT using OpenView software written and kindly provided by N.E. Ziv (Tsurriel et al, 2006). Mean IF intensities were measured in synaptic ROIs in all corresponding channels using the same software and normalised to the mean IF intensities of the control group in each experiment. For analyses of active synapses, puncta with over-threshold staining for Syn1 and VGLUT1 or VGAT were considered as excitatory or inhibitory synapses.

Synaptotagmin1 antibody uptake

For quantitative assessment, all coverslips compared in one experiment were processed in parallel using identical antibodies solutions and other reagents as described earlier (Lazarevic et al, 2011). For the Syt1Ab uptake, neurons grown for 19–21 days *in vitro* (DIV) were washed with Tyrode's buffer (TB) containing: 119 mM NaCl, 2.5 mM KCl, 2 mM CaCl₂, 2 mM MgCl₂, 30 mM glucose and 25 mM HEPES, pH 7.4, and then incubated with Oyster 550-labelled antibody against the luminal domain of Syt1. To monitor endogenous network activity-induced Syt1Ab uptake neurons were incubated with Oyster 550-labelled anti Syt1 antibody in TB for 20 min at 37°C. To visualise all release-competent vesicles Oyster 550-labelled anti Syt1 antibody was applied to cells in high K⁺ TB containing 71.5 mM NaCl, 50 mM KCl, 2 mM CaCl₂, 2 mM MgCl₂, 30 mM glucose and 25 mM HEPES, pH 7.4 for 4 min. Then, cells were washed twice with TB, fixed with 4% (w/v) PFA, permeabilized with 0.3% (v/v) Triton X-100 and stained with specific antibodies as described earlier (Lazarevic et al, 2011). Synapses with over-threshold IF for Syt1Ab uptake were considered as active synapses.

Lentiviral particles production

The lentiviral vector for expression of ratio:sypHy (Rose et al, 2013) was described in (Lazarevic et al, 2017). Lentiviral particles were generated in HEK293T cells (ATTC, Manassas, VA, USA) using psPAX2 packaging and pVSVG pseudotyping vectors (Lois et al, 2002). HEK293T cells were grown in media containing 10% (v/v) FCS to 60% confluence in the 75 cm² flasks. Cells were transfected with 20 µg of total DNA per flask using the calcium phosphate method (Fejtova et al, 2009). The molar ratio of FUGW: psPAX2: pVSVG was 4:2:1. 6–8 h after transfection, the medium was changed to 10 ml production medium containing Neurobasal A supplemented with antibiotics, 1 mM sodium pyruvate (Life Technologies), B27 and 1 mM GlutaMAX™ (Life Technologies). 48 h after transfection, virus-containing media was collected and cleared off large cellular debris by centrifugation for 20 min at 2,000 g. Virus-containing supernatant was aliquoted and stored at –80°C.

SynaptopHluorin (sypHy) imaging

Imaging experiments for the assessment of RRP and TRP were carried out in 19–20 DIV hippocampal neurons. Cells were transduced with the lentiviral particles expressing ratio:sypHy at days 3–4. Transduced neurons were identified by their RFP expression. Coverslips were mounted in a chamber equipped with field stimulation electrodes (RC-49MFSH; Warner instruments). Electrical stimulation was generated using an isolator unit (WPI) controlled by Master-8 pulse generator (AMPI). During the whole experiment, cells were kept in TB supplemented with 50 µM APV and 25 µM CNQX to avoid the recurrent network activity-driven release and with 1 µM of Bafilomycin A to prevent the vesicle re-acidification of once released vesicles (Sankaranarayanan & Ryan, 2001). Imaging experiments were done at RT on an inverted microscope (Zeiss Axio Observer.A1) using 63× oil immersion objective (NA 1.4) and GFP/mCherry ET filter set (single-band excitors 470/40 and 572/35, dichroic Chroma #59022BS, emitter Chroma #59022m). Images were acquired at a frame rate of 12 Hz using an EMCCD camera (Evolve 512; Photometrics) controlled by VisiView (Visitron Systems GmbH). After 5 s of baseline acquisition (F₀), neurons were stimulated with 40 AP at 20 Hz to release of RRP. After 2 min recovery time, TRP was released by application of 900 AP at 20 Hz, 1 min later a pulse of TB containing 60 mM NH₄Cl was applied to visualise all sypHy-expressing vesicles (Burrone et al, 2006).

Analysis was done using established routines and without knowing the genotype and treatments. The first background (calculated from four independent background regions within the image) was mathematically subtracted. Responding synaptic puncta were visualised by subtracting the first 10 frames corresponding to the baseline from the traces obtained directly after the 900 AP stimulus. Circular ROIs with a diameter of 8 × 8 pixels were placed over each responding bouton and mean IF values from between 80 and 150 ROIs per visual field were measured using the Time Series Analyser V2.0 plugin in ImageJ (NIH, <http://rsb.info.nih.gov/ij/>). Only the boutons showing stable responses and TRP ≤ 80% of NH₄Cl-evoked fluorescence were considered for the analyses. Bleaching correction was done by normalising the bleaching factor obtained from imaging experiments without stimulation performed on the same coverslip. Traces were plotted using GraphPad software. The relative

sizes of the RRP and the TRP were expressed as fractions of the total synHy-expressing pool detected after the addition of NH_4Cl ($F_{\text{NH}_4\text{Cl}}$). RRP and TRP were quantified by averaging the mean of 100 values per ROI plateau phases (frames 150–250 corresponding to time points between 10 and 20 s after the start of image acquisition and 600–700 corresponding to time points \approx 165–175 s, respectively, on the XY graph). ResP was quantified as $F_{\text{NH}_4\text{Cl}} - F_{\text{TRP}}$.

Brain fractionation and quantitative Western blot

For WBs for pSer9Syn1 and pSer551Syn1 10–18 weeks old animals, for all remaining immunoblots and activity assays 8 weeks old WT and Bsn^{GT} littermates of both sexes were used. Hippocampi were isolated and if necessary snap frozen at -80°C till further processing. Tissue was homogenised in buffer containing 25 mM Tris-HCl pH 7.4, 0.32 M sucrose supplemented with Complete mini protease inhibitors (# 11836153001, Roche), PhosStop phosphatase inhibitor cocktail (# 4906837001, Roche) using Potter glass-Teflon homogeniser (B. Braun International) with 12 strokes at 900 rpm. Cell debris and nuclei were sedimented at 1,000 g for 10 min at 4°C . The supernatant was collected and centrifuged again at 12,000 g for 20 min at 4°C to obtain supernatant (S2) corresponding to the cytoplasmic fraction and pellet (P2) corresponding to the crude membrane fraction. Protein concentrations in fractions were determined using the BC assay (# UP40840A, Interchim).

To obtain samples for Western blotting, the P2 pellet was resuspended in 25 mM Tris-HCl, pH 7.4, 150 mM NaCl, 1% (v/v) Triton X-100 supplemented with Complete mini protease inhibitors and PhosStop phosphatase inhibitor cocktail. An equal amount of proteins (20 $\mu\text{g}/\text{lane}$) were separated using one-dimensional SDS-PAGE and then transferred to Millipore Immobilon-FL PVDF membranes. For immunodetection, the primary antibody was applied at 4°C overnight and the fluorescently labelled secondary antibodies for 1 h at room temperature. Antibodies were diluted in PBS containing 0.1% (v/v) Tween 20, 5% (w/v) BSA and 0.025% (w/v) sodium azide. Immunodetection was carried out using a chemiluminescent imager for quantification of pSer145PDE4B and PDE4B immunoreactivity and using Odyssey Infrared Imagine System and Odyssey software v2.1 (Li-COR) for all other experiments. Quantification of the blots was performed using ImageJ software. After background subtraction, the IF of phosphorylated SNAP25, PDE4 or Syn1 were normalised to IF of total respective proteins measured on the same immunoblot in the alternative channel or in the case of SNAP25 and PDE4 after membrane stripping using RestoreTM stripping buffer (# 46428, Pierce). The immunoreactivity of Syn1 was normalised to total protein stain visualised using No-stainTM protein labelling reagent (#A44449, Thermo Fischer) of the respective sample.

Measurement of PKA activity

P2 pellets were prepared from hippocampi of 8 weeks old animals as described above and resuspended in a buffer containing 25 mM Tris-HCl pH 7.4, 150 mM NaCl, 0.5% (v/v) Triton X100 and Complete mini protease and PhosStop phosphatase inhibitor cocktail. Samples containing equal protein amount, as assessed by BC assay (#UP40840A, Interchim), were incubated with GammaBind Plus

Sepharose beads (#GE17-0886-02, GE Healthcare) coupled with rabbit polyclonal antibody against PKA α cat (C-20; Santa Cruz Biotechnology) for 4 h at 4°C . After washing three times with PKA assay buffer (40 mM Tris pH 7.5, 20 mM MgCl_2 , 0.1 mg BSA, 0.1 mM DTT) the immunoprecipitates were resuspended in 50 μl of the same buffer supplemented with 70 μM ATP and 0.3 mM Kemptide, a PKA substrate (LRRASLG; # V5601 Promega) and incubated for 0.5 h at 30°C in 96-well plate. The ATP hydrolysis was detected upon the addition of 50 $\mu\text{l}/\text{well}$ luminescent Kinase Glo plus reagent (# V6711, Promega) using FLUOstar Omega microplate reader (BMG Labtech).

Calcineurin activity assay

Calcineurin activity was assessed using Calcineurin activity assay kit (#20700, Calbiochem). Hippocampus tissue of 8 weeks old animals was homogenised in the lysis buffer (25 mM Tris-HCl pH 7.5, 50 μM EDTA, 50 μM EGTA, 0.2% (v/v) Nonidet P-40, 0.5 mM dithiothreitol, Complete mini protease inhibitors) by gently pressing through 16G needle. Homogenates were cleared by centrifugation at 100,000 g at 4°C for 45 min. Protein concentration was assessed by BC assay, and samples with an equal protein amount were processed for the assay. Free phosphate was removed, samples were rebuffed to the assay buffer containing 100 mM NaCl, 50 mM Tris-HCl (pH 7.5), 6 mM MgCl_2 , 0.5 mM CaCl_2 , 0.5 mM dithiothreitol, 0.05% (v/v) Nonidet P-40 and incubated with RII phosphopeptide DLDVPIPIGRFDRRVpSVAEE, a specific calcineurin substrate, for 0.5 h at 30°C in a 96-well plate. The phosphate release was detected upon the addition of 100 $\mu\text{l}/\text{well}$ of Green reagent by absorbance measurement at 620 nm. The Ca^{2+} -independent phosphatase activity was measured in samples supplemented with EGTA and subtracted from measured values to obtain calcineurin phosphatase activity.

cAMP assay

P2 pellets were prepared from hippocampi of 8 weeks old animals as described above and dissolved in a buffer containing 0.1 M HCl and 0.5% Triton-X 100. The cAMP levels in samples containing equal protein concentrations were quantified using ELISA-based assay kit (#ADI-900-163, ENZO Life Sciences). The assay was done following the manufacturer's instructions.

PDE4 immunoprecipitation and activity assay

PDE4 activity was assessed using a cyclic nucleotide phosphodiesterase assay kit (#BML- AK800-0001, Enzo Life Sciences) according to the supplier's instructions. In brief, hippocampal crude membrane pellets P2 prepared as described above were resuspended with ice-cold buffer containing 50 mM HEPES pH 7.4, 120 mM NaCl, 0.1 mM EDTA, 0.5% (v/v) Triton X-100 and Complete mini protease inhibitors (Roche). Upon removal of free phosphate, samples containing the same protein amount were subjected to immunoprecipitation with rabbit polyclonal antibody against PDE4B (H-56) (#sc-25812, Santa Cruz Biotechnology) coupled to GammaBind Plus Sepharose beads (# 17-0886-02, GE Healthcare) for 4 h at 4°C . After three times washing with PDE assay buffer (10 mM Tris-HCl, pH 7.4), immunoprecipitates were resuspended

in 50 μ l of the same buffer supplemented with 0.2 mM 3',5'-cAMP substrate and 5'-nucleotidase enzyme (50 kU/well) and incubated for 0.5 h at 30°C in a 96-well plate. Phosphate release was detected upon incubation with Green reagent (100 μ l/per well) for 30 min by measurement of absorbance at 620 nm in a microplate-reading spectrophotometer.

Statistical analysis

All results of quantitative analyses are given as means \pm standard errors of the mean (SEM). Statistical analyses were performed with Prism 9 software (GraphPad Software, Inc.) using the Student's *t*-test, one-way or two-way ANOVA as indicated for each experiment. Statistical assumptions (i.e. normal distribution) were tested before the application of the appropriate test. Statistical significance is marked as **P* < 0.05, ***P* < 0.01, ****P* < 0.001 in all plots. Information about group character and size is specified in the figure legend for each experiment and summarised in Table EV1.

Data availability

This study includes no data deposited in public repositories.

Expanded View for this article is available online.

Acknowledgements

We thank Janina Juhle, Isabel Herbert, Kati Ebert, Juliana Monti, Sabine Müller, Peggy Patella and the animal facility at LIN Magdeburg and PETZ Erlangen for excellent technical assistance. We also acknowledge Anna Fassio, Fabio Benfenati, James A. Bibb and Miles D. Housley for generously providing the noncommercial antibodies used in this study. This study was supported by DFG (FE1335/3) and BMBF GeNeRARE (FZ O1GM1902B) to AF, ERANET/BMBF (AMRe-PACELL) and BMBF 01DN17002 (Preplastic) to EDG, Center for Behavioural Brain Sciences—CBBS promoted by Europäische Fonds für regionale Entwicklung—EFRE (ZS/2016/04/78113) to CMV. Open Access funding enabled and organized by Projekt DEAL.

Author contributions

Carolina Montenegro-Venegas: Conceptualization; data curation; formal analysis; supervision; funding acquisition; investigation; visualization; methodology; project administration. **Debarpan Guhathakurta:** Investigation; visualization. **Eneko Pina-Fernandez:** Methodology. **Maria Andres-Alonso:** Methodology. **Florian Plattner:** Resources; investigation. **Eckart D Gundelfinger:** Resources; funding acquisition. **Anna Fejtova:** Conceptualization; resources; data curation; formal analysis; supervision; funding acquisition; visualization; project administration.

In addition to the [CRediT](#) author contributions listed above, the contributions in detail are:

CMV and AF performed conceptualization, supervision, formal analysis, project administration, data curation and writing—original draft; CMV, DG and FP involved in investigation; CMV, DG, EPF, MAA, FP and AF involved in methodology; CMV, EDG and AF involved in funding acquisition; EDG and AF involved in resources; CMV, DG and AF involved in visualisation; all authors involved in writing—review and editing.

Disclosure and competing interests statement

The authors declare that they have no conflict of interest.

References

- Ackermann F, Schink KO, Bruns C, Izsavak Z, Hamra FK, Rosenmund C, Garner CC (2019) Critical role for piccolo in synaptic vesicle retrieval. *elife* 8: e46629
- Alabi AA, Tsien RW (2012) Synaptic vesicle pools and dynamics. *Cold Spring Harb Perspect Biol* 4: a013680
- Altmüller F, Pothula S, Annamneedi A, Nakhaei-Rad S, Montenegro-Venegas C, Pina-Fernandez E, Marini C, Santos M, Schanze D, Montag D et al (2017) Aberrant neuronal activity-induced signaling and gene expression in a mouse model of RASopathy. *PLoS Genet* 13: e1006684
- Altrock WD, tom Dieck S, Sokolov M, Meyer AC, Sigler A, Brakebusch C, Fassler R, Richter K, Boeckers TM, Potschka H et al (2003) Functional inactivation of a fraction of excitatory synapses in mice deficient for the active zone protein bassoon. *Neuron* 37: 787–800
- Babai N, Gierke K, Müller T, Regus-Leidig H, Brandstätter JH, Feigenspan A (2019) Signal transmission at invaginating cone photoreceptor synaptic contacts following deletion of the presynaptic cytomatrix protein Bassoon in mouse retina. *Acta Physiol* 226: e13241
- Babai N, Wittgenstein J, Gierke K, Brandstätter JH, Feigenspan A (2021) The absence of functional bassoon at cone photoreceptor ribbon synapses affects signal transmission at Off cone bipolar cell contacts in mouse retina. *Acta Physiol* 231: e13584
- Bonnycastle K, Davenport EC, Cousin MA (2020) Presynaptic dysfunction in neurodevelopmental disorders: insights from the synaptic vesicle life cycle. *J Neurochem* 157: 179–207
- Buran BN, Strenzke N, Neef A, Gundelfinger ED, Moser T, Liberman MC (2010) Onset coding is degraded in auditory nerve fibers from mutant mice lacking synaptic ribbons. *J Neurosci* 30: 7587–7597
- Burrone J, Li Z, Murthy VN (2006) Studying vesicle cycling in presynaptic terminals using the genetically encoded probe synaptopHluorin. *Nat Protoc* 1: 2970–2978
- Cesca F, Baldelli P, Valtorta F, Benfenati F (2010) The synapsins: Key actors of synapse function and plasticity. *Prog Neurobiol* 91: 313–348
- Chanaday NL, Cousin MA, Milosevic I, Watanabe S, Morgan JR (2019) The synaptic vesicle cycle revisited: New insights into the modes and mechanisms. *J Neurosci* 39: 8209–8216
- Chen C, Regehr WG (1997) The mechanism of cAMP-mediated enhancement at a cerebellar synapse. *J Neurosci* 17: 8687–8694
- Chenouard N, Xuan F, Tsien RW (2020) Synaptic vesicle traffic is supported by transient Actin filaments and regulated by PKA and NO. *Nat Commun* 11: 5318
- Chi P, Greengard P, Ryan TA (2003) Synaptic vesicle mobilization is regulated by distinct synapsin I phosphorylation pathways at different frequencies. *Neuron* 38: 69–78
- Davydova D, Marini C, King C, Klueva J, Bischof F, Romorini S, Montenegro-Venegas C, Heine M, Schneider R, Schroder MS et al (2014) Bassoon specifically controls presynaptic P/Q-type Ca²⁺ channels via RIM-binding protein. *Neuron* 82: 181–194
- Denker A, Rizzoli SO (2010) Synaptic vesicle pools: an update. *Front Synaptic Neurosci* 2: 135
- Dick O, tom Dieck S, Altrock WD, Ammermüller J, Weiler R, Garner CC, Gundelfinger ED, Brandstätter JH (2003) The presynaptic active zone protein bassoon is essential for photoreceptor ribbon synapse formation in the retina. *Neuron* 37: 775–786
- Dieck S, Sanmartí-Vila L, Langnaese K, Richter K, Kindler S, Soyke A, Wex H, Smalla K-H, Kämpf I, Fränzer J-T et al (1998) Bassoon, a novel zinc-finger CAG/glutamine-repeat protein selectively localized at the active zone of presynaptic nerve terminals. *J Cell Biol* 142: 499–509

- Engholm-Keller K, Waardenberg AJ, Muller JA, Wark JR, Fernando RN, Arthur JW, Robinson PJ, Dietrich D, Schoch S, Graham ME (2019) The temporal profile of activity-dependent presynaptic phospho-signalling reveals long-lasting patterns of poststimulus regulation. *PLoS Biol* 17: e3000170
- Fejtova A, Davydova D, Bischof F, Lazarevic V, Altmann WD, Romorini S, Schone C, Zuschratter W, Kreutz MR, Garner CC et al (2009) Dynein light chain regulates axonal trafficking and synaptic levels of bassoon. *J Cell Biol* 185: 341–355
- Frank T, Rutherford MA, Strenzke N, Neef A, Pangrsić T, Khimich D, Fejtova A, Gundelfinger ED, Liberman MC, Harke B et al (2010) Bassoon and the synaptic ribbon organize Ca²⁺ channels and vesicles to add release sites and promote refilling. *Neuron* 68: 724–738
- Fu H, Subramanian RR, Masters SC (2000) 14-3-3 proteins: Structure, function, and regulation. *Annu Rev Pharmacol Toxicol* 40: 617–647
- Guan JS, Su SC, Gao J, Joseph N, Xie Z, Zhou Y, Durak O, Zhang L, Zhu JJ, Clauser KR et al (2011) Cdk5 is required for memory function and hippocampal plasticity via the cAMP signaling pathway. *PLoS One* 6: e25735
- Gundelfinger ED, Reissner C, Garner CC (2015) Role of bassoon and piccolo in assembly and molecular organization of the active zone. *Front Synaptic Neurosci* 7: 19
- Hallermann S, Fejtova A, Schmidt H, Weyhersmuller A, Silver RA, Gundelfinger ED, Eilers J (2010) Bassoon speeds vesicle reloading at a central excitatory synapse. *Neuron* 68: 710–723
- Harata N, Ryan TA, Smith SJ, Buchanan J, Tsien RW (2001) Visualizing recycling synaptic vesicles in hippocampal neurons by FM 1-43 photoconversion. *Proc Natl Acad Sci USA* 98: 12748–12753
- Hoffmann-Conaway S, Brockmann MM, Schneider K, Annamneedi A, Rahman KA, Bruns C, Textoris-Taube K, Trimbuch T, Smalla KH, Rosenmund C et al (2020) Parkin contributes to synaptic vesicle autophagy in bassoon-deficient mice. *elife* 9: e56590
- Huang YY, Li XC, Kandel ER (1994) cAMP contributes to mossy fiber LTP by initiating both a covalently mediated early phase and macromolecular synthesis-dependent late phase. *Cell* 79: 69–79
- Huston E, Lumb S, Russell A, Catterall C, Ross AH, Steele MR, Bolger GB, Perry MJ, Owens RJ, Houslay MD (1997) Molecular cloning and transient expression in COS7 cells of a novel human PDE4B cAMP-specific phosphodiesterase, HSPDE4B3. *Biochem J* 328 (Pt 2): 549–558
- Huttner WB, DeGennaro LJ, Greengard P (1981) Differential phosphorylation of multiple sites in purified protein I by cyclic AMP-dependent and calcium-dependent protein kinases. *J Biol Chem* 256: 1482–1488
- Jing Z, Rutherford MA, Takago H, Frank T, Fejtova A, Khimich D, Moser T, Strenzke N (2013) Disruption of the presynaptic cytomatrix protein bassoon degrades ribbon anchorage, multiquantal release, and sound encoding at the hair cell afferent synapse. *J Neurosci* 33: 4456–4467
- Kaech S, Huang CF, Banker G (2012) General considerations for live imaging of developing hippocampal neurons in culture. *Cold Spring Harb Protoc* 2012: 312–318
- Khimich D, Nouvian R, Pujol R, tom Dieck S, Egnér A, Gundelfinger ED, Moser T (2005) Hair cell synaptic ribbons are essential for synchronous auditory signalling. *Nature* 434: 889–894
- Kim SH, Ryan TA (2010) CDK5 serves as a major control point in neurotransmitter release. *Neuron* 67: 797–809
- Kim SH, Ryan TA (2013) Balance of calcineurin A α and CDK5 activities sets release probability at nerve terminals. *J Neurosci* 33: 8937–8950
- Kim NS, Wen Z, Liu J, Zhou Y, Guo Z, Xu C, Lin YT, Yoon KJ, Park J, Cho M et al (2021) Pharmacological rescue in patient iPSC and mouse models with a rare DISC1 mutation. *Nat Commun* 12: 1398
- Kohansal-Nodehi M, Chua JJ, Urlaub H, Jahn R, Czernik D (2016) Analysis of protein phosphorylation in nerve terminal reveals extensive changes in active zone proteins upon exocytosis. *elife* 5: e14530
- Kraszewski K, Mundigl O, Daniell L, Verderio C, Matteoli M, De Camilli P (1995) Synaptic vesicle dynamics in living cultured hippocampal neurons visualized with CY3-conjugated antibodies directed against the luminal domain of synaptotagmin. *J Neurosci* 15: 4328–4342
- Lazarevic V, Schone C, Heine M, Gundelfinger ED, Fejtova A (2011) Extensive remodeling of the presynaptic cytomatrix upon homeostatic adaptation to network activity silencing. *J Neurosci* 31: 10189–10200
- Lazarevic V, Fienko S, Andres-Alonso M, Anni D, Ivanova D, Montenegro-Venegas C, Gundelfinger ED, Cousin MA, Fejtova A (2017) Physiological concentrations of amyloid Beta regulate recycling of synaptic vesicles via Alpha7 acetylcholine receptor and CDK5/calcineurin signaling. *Front Mol Neurosci* 10: 221
- Lois C, Hong EJ, Pease S, Brown EJ, Baltimore D (2002) Germline transmission and tissue-specific expression of transgenes delivered by lentiviral vectors. *Science* 295: 868–872
- Lonart G, Janz R, Johnson KM, Sudhof TC (1998) Mechanism of action of rab3A in mossy fiber LTP. *Neuron* 21: 1141–1150
- MacKenzie SJ, Baillie GS, McPhee I, MacKenzie C, Seamons R, McSorley T, Millen J, Beard MB, van Heeke G, Houslay MD (2002) Long PDE4 cAMP specific phosphodiesterases are activated by protein kinase A-mediated phosphorylation of a single serine residue in upstream conserved region 1 (UCR1). *Br J Pharmacol* 136: 421–433
- Mendoza Schulz A, Jing Z, Sanchez Caro JM, Wetzel F, Dresbach T, Strenzke N, Wichmann C, Moser T (2014) Bassoon-disruption slows vesicle replenishment and induces homeostatic plasticity at a CNS synapse. *EMBO J* 33: 512–527
- Menegon A, Bonanomi D, Albertinazzi C, Lotti F, Ferrari G, Kao HT, Benfenati F, Baldelli P, Valtorta F (2006) Protein kinase A-mediated synapsin I phosphorylation is a central modulator of Ca²⁺-dependent synaptic activity. *J Neurosci* 26: 11670–11681
- Millar JK, Pickard BS, Mackie S, James R, Christie S, Buchanan SR, Malloy MP, Chubb JE, Huston E, Baillie GS et al (2005) DISC1 and PDE4B are interacting genetic factors in schizophrenia that regulate cAMP signaling. *Science* 310: 1187–1191
- Montenegro-Venegas C, Fienko S, Anni D, Pina-Fernandez E, Frischknecht R, Fejtova A (2021) Bassoon inhibits proteasome activity via interaction with PSMB4. *Cell Mol Life Sci* 78: 1545–1563
- Moulder KL, Jiang X, Chang C, Taylor AA, Benz AM, Conti AC, Muglia LJ, Mennerick S (2008) A specific role for Ca²⁺-dependent adenylyl cyclases in recovery from adaptive presynaptic silencing. *J Neurosci* 28: 5159–5168
- Moulder KL, Jiang X, Taylor AA, Benz AM, Mennerick S (2010) Presynaptically silent synapses studied with light microscopy. *J Vis Exp* 35: 1676
- Mukherjee K, Yang X, Gerber SH, Kwon HB, Ho A, Castillo PE, Liu X, Sudhof TC (2010) Piccolo and bassoon maintain synaptic vesicle clustering without directly participating in vesicle exocytosis. *Proc Natl Acad Sci USA* 107: 6504–6509
- Nagy G, Reim K, Matti U, Brose N, Binz T, Rettig J, Neher E, Sorensen JB (2004) Regulation of releasable vesicle pool sizes by protein kinase A-dependent phosphorylation of SNAP-25. *Neuron* 41: 417–429
- Park H, Lee JA, Lee C, Kim MJ, Chang DJ, Kim H, Lee SH, Lee YS, Kaang BK (2005) An Aplysia type 4 phosphodiesterase homolog localizes at the presynaptic terminals of Aplysia neuron and regulates synaptic facilitation. *J Neurosci* 25: 9037–9045
- Patzke C, Brockmann MM, Dai J, Gan KJ, Grauel MK, Fenske P, Liu Y, Acuna C, Rosenmund C, Sudhof TC (2019) Neuromodulator signaling bidirectionally controls vesicle numbers in human synapses. *Cell* 179: e422

- Patzke C, Dai J, Brockmann MM, Sun Z, Fenske P, Rosenmund C, Sudhof TC (2021) Cannabinoid receptor activation acutely increases synaptic vesicle numbers by activating synapsins in human synapses. *Mol Psychiatry* 26: 6253–6268
- Pieribone VA, Shupliakov O, Brodin L, Hilfiker-Rothenfluh S, Czernik AJ, Greengard P (1995) Distinct pools of synaptic vesicles in neurotransmitter release. *Nature* 375: 493–497
- Plattner F, Hayashi K, Hernandez A, Benavides DR, Tassin TC, Tan C, Day J, Fina MW, Yuen EY, Yan Z *et al* (2015) The role of ventral striatal cAMP signaling in stress-induced behaviors. *Nat Neurosci* 18: 1094–1100
- Risinger C, Bennett MK (1999) Differential phosphorylation of syntaxin and synaptosome-associated protein of 25 kDa (SNAP-25) isoforms. *J Neurochem* 72: 614–624
- Rizzoli SO, Betz WJ (2005) Synaptic vesicle pools. *Nat Rev Neurosci* 6: 57–69
- Rose T, Schoenenberger P, Jezek K, Oertner TG (2013) Developmental refinement of vesicle cycling at Schaffer collateral synapses. *Neuron* 77: 1109–1121
- Ryl M, Urbasik A, Gierke K, Babai N, Joachimsthaler A, Feigenspan A, Frischknecht R, Stallwitz N, Fejtova A, Kremers J *et al* (2021) Genetic disruption of bassoon in two mutant mouse lines causes divergent retinal phenotypes. *FASEB J* 35: e21520
- Sankaranarayanan S, Ryan TA (2001) Calcium accelerates endocytosis of vSNAREs at hippocampal synapses. *Nat Neurosci* 4: 129–136
- Shikorski T, Stevens CF (2001) Morphological correlates of functionally defined synaptic vesicle populations. *Nat Neurosci* 4: 391–395
- Schroder MS, Stellmacher A, Romorini S, Marini C, Montenegro-Venegas C, Altrrock WD, Gundelfinger ED, Fejtova A (2013) Regulation of presynaptic anchoring of the scaffold protein bassoon by phosphorylation-dependent interaction with 14-3-3 adaptor proteins. *PLoS One* 8: e58814
- Silbern I, Pan KT, Fiosins M, Bonn S, Rizzoli SO, Fornasiero EF, Urlaub H, Jahn R (2021) Protein phosphorylation in depolarized Synaptosomes: dissecting primary effects of calcium from synaptic vesicle cycling. *Mol Cell Proteomics* 20: 100061
- Su SC, Seo J, Pan JQ, Samuels BA, Rudenko A, Ericsson M, Neve RL, Yue DT, Tsai LH (2012) Regulation of N-type voltage-gated calcium channels and presynaptic function by cyclin-dependent kinase 5. *Neuron* 75: 675–687
- Sudhof TC (2004) The synaptic vesicle cycle. *Annu Rev Neurosci* 27: 509–547
- Torres-Quesada O, Mayrhofer JE, Stefan E (2017) The many faces of compartmentalized PKA signalosomes. *Cell Signal* 37: 1–11
- Truckenbrodt S, Viplav A, Jahne S, Vogts A, Denker A, Wildhagen H, Fornasiero EF, Rizzoli SO (2018) Newly produced synaptic vesicle proteins are preferentially used in synaptic transmission. *EMBO J* 37: e98044
- Tsuriel S, Geva R, Zamorano P, Dresbach T, Boeckers T, Gundelfinger ED, Garner CC, Ziv NE (2006) Local sharing as a predominant determinant of synaptic matrix molecular dynamics. *PLoS Biol* 4: e271
- Vaden JH, Banumurthy G, Gusarevich ES, Overstreet-Wadiche L, Wadiche JI (2019) The readily-releasable pool dynamically regulates multivesicular release. *elife* 8: e47434
- Valente P, Casagrande S, Nieuw T, Versteegen AM, Valtorta F, Benfenati F, Baldelli P (2012) Site-specific synapsin I phosphorylation participates in the expression of post-tetanic potentiation and its enhancement by BDNF. *J Neurosci* 32: 5868–5879
- Versteegen AM, Tagliatti E, Lignani G, Marte A, Stoloro T, Atias M, Corradi A, Valtorta F, Gitler D, Onofri F *et al* (2014) Phosphorylation of synapsin I by cyclin-dependent kinase-5 sets the ratio between the resting and recycling pools of synaptic vesicles at hippocampal synapses. *J Neurosci* 34: 7266–7280
- Waites CL, Leal-Ortiz SA, Okerlund N, Dalke H, Fejtova A, Altrock WD, Gundelfinger ED, Garner CC (2013) Bassoon and piccolo maintain synapse integrity by regulating protein ubiquitination and degradation. *EMBO J* 32: 954–969
- Wiescholleck V, Manahan-Vaughan D (2012) PDE4 inhibition enhances hippocampal synaptic plasticity in vivo and rescues MK801-induced impairment of long-term potentiation and object recognition memory in an animal model of psychosis. *Transl Psychiatry* 2: e89



License: This is an open access article under the terms of the Creative Commons Attribution-NonCommercial-NoDerivs License, which permits use and distribution in any medium, provided the original work is properly cited, the use is non-commercial and no modifications or adaptations are made.